NIH Public Access
Author Manuscript
Exp Neurol. Author manuscript; available in PMC 2015 May 01.

Published in final edited form as:
Exp Neurol. 2014 May ; 255: 113–126. doi:10.1016/j.expneurol.2014.02.025.

Changes in NG2 cells and oligodendrocytes in a new model of intraspinal hemorrhage

F. Rezan Sahinkaya[1,2,3], **Lindsay Milich**[3], and **Dana M. McTigue**[1,3]

[1]Department of Neuroscience, Ohio State University, Columbus, OH 43210

[2]Neuroscience Graduate Studies Program, Ohio State University, Columbus, OH 43210

[3]Center for Brain and Spinal Cord Repair, Ohio State University, Columbus, OH 43210

Abstract

Spinal cord injury (SCI) evokes rapid deleterious and reparative glial reactions. Understanding the triggers for these responses is necessary for designing strategies to maximize repair. This study examined lesion formation and glial responses to vascular disruption and hemorrhage, a prominent feature of acute SCI. The specific role of hemorrhage is difficult to evaluate in trauma-induced lesions, because mechanical injury initiates many downstream responses. To isolate vascular disruption from trauma-induced effects, we created a novel and reproducible model of collagenase-induced intraspinal hemorrhage (ISH) and compared glial reactions between unilateral ISH and a hemi-contusion injury. Similar to contusion injuries, ISH lesions caused loss of myelin and axons and became filled with iron-laden macrophages. We hypothesized that intraspinal hemorrhage would also initiate reparative cellular responses including NG2+ oligodendrocyte progenitor cell (OPC) proliferation and oligodendrocyte genesis. Indeed, ISH induced OPC proliferation within 1d post-injury (dpi), which continued throughout the first week and resulted in a sustained elevation of NG2+ OPCs. ISH also caused oligodendrocyte loss within 4h that was sustained through 3d post-ISH. However, oligodendrogenesis, as determined by bromo-deoxyuridine (BrdU) positive oligodendrocytes, restored oligodendrocyte numbers by 7dpi, revealing that proliferating OPCs differentiated into new oligodendrocytes after ISH. The signaling molecules pERK1/2 and pSTAT3 were robustly increased acutely after ISH, with pSTAT3 being expressed in a portion of OPCs, suggesting that activators of this signaling cascade may initiate OPC responses. Aside from subtle differences in timing of OPC responses, changes in ISH tissue closely mimicked those in hemi-contusion tissue. These results are important for elucidating the contribution of hemorrhage to lesion formation and endogenous cell-mediated repair, and will provide the foundation for future studies geared toward identifying the role of specific blood components on injury and repair mechanisms. This understanding may provide new clinical targets for SCI and other devastating conditions such as intracerebral hemorrhage.

© 2014 Elsevier Inc. All rights reserved.

[1]**Corresponding author**: Dana M. McTigue, PhD, Department of Neuroscience, 692 Biomedical Research Tower, 460 W 12th Ave, Columbus, OH 43210, Mctigue.2@osu.edu, 614-292-5523.

Publisher's Disclaimer: This is a PDF file of an unedited manuscript that has been accepted for publication. As a service to our customers we are providing this early version of the manuscript. The manuscript will undergo copyediting, typesetting, and review of the resulting proof before it is published in its final citable form. Please note that during the production process errors may be discovered which could affect the content, and all legal disclaimers that apply to the journal pertain.

NIH-PA Author Manuscript
NIH-PA Author Manuscript
NIH-PA Author Manuscript

NIH-PA Author Manuscript

NIH-PA Author Manuscript

NIH-PA Author Manuscript

Keywords

myelin; progenitor; spinal cord injury; gliogenesis; inflammation; iron; blood

Introduction

Traumatic spinal cord injury (SCI) induces a complex cascade of secondary injury events (e.g., bleeding, ischemia, inflammation, excitotoxicity, etc.) that together damage neural tissue or impede mechanisms of repair. The complexity of these cascades, including their overlapping temporal profiles and redundant cellular targets, make it difficult to decipher the relative contribution of any single component to injury/repair after SCI. Conversely, simplified "reductionist" *in vivo* models can be useful tools for revealing how changes to individual cellular or molecular pathways affect secondary injury or central nervous system (CNS) repair. For example, we previously developed and characterized different models of intraspinal inflammation that revealed different modes of microglia/macrophage activation had distinct effects on neuron survival, oligodendrogenesis, axotomy and axon regeneration (Popovich et al., 2002; Schonberg et al., 2007; Gensel et al., 2009; Kigerl et al., 2012; Schonberg et al., 2012). In each case, these models focus on changes that likely develop several days after traumatic SCI, corresponding with the onset of monocyte infiltration. Missing is a robust and reproducible model to predict the unique contributions of bleeding to the early phases of CNS injury. Indeed, mechanical injury to the spinal cord rapidly damages the spinal microvasculature resulting in acute intraspinal bleeding with progressive hemorrhagic necrosis (PHN), which is highly destructive. In fact, interventions that prevent or reduce PHN after SCI are markedly protective (Noble and Wrathall, 1989a; 1989b; Hill, 2001; Simard et al., 2007; 2010; Benton and Hagg, 2011; Popovich et al., 2011; Simard et al., 2012; 2013). However, bleeding can have conflicting effects on glia, especially oligodendrocyte lineage cells. *In vitro* data show that plasma and serum are toxic to NG2+ oligodendrocyte progenitors (OPCs) (Juliet et al., 2009), while *in vivo* data show that blood-brain barrier breakdown or microinjecting platelets or whole blood into intact brain increases NG2 immunoreactivity (Rhodes et al., 2006). A similar effect on NG2+ OPCs was found by selectively activating macrophages in a microenvironment similar to that present after ischemic or traumatic injury with bleeding (Kigerl et al., 2012).

One of the best-characterized functions of OPCs (also known as polydendrocytes) is to provide a source for new oligodendrocytes during development, aging and after CNS demyelination or injury (McTigue et al., 2001; Watanabe et al., 2002; Zai and Wrathall, 2005; Horky et al., 2006; Tripathi and McTigue, 2007; Zhu et al., 2008; Psachoulia et al., 2010). Upon traumatic injury, OPCs undergo robust and protracted proliferation, accumulate along the lesion borders, and infiltrate into the lesion proper where they continually increase in number and closely associate with axons (McTigue et al., 2006; Busch et al., 2010). Despite migration and proliferation of OPCs around and into traumatic lesions, differentiation into new oligodendrocytes only occurs in the lesion border and spared tissue (McTigue et al., 2006; Tripathi and McTigue, 2007). In fact, robust oligodendrocyte generation in lesion borders after spinal contusion results in greater oligodendrocyte numbers compared to uninjured tissue (Tripathi and McTigue, 2007). The signals that

NIH-PA Author Manuscript

NIH-PA Author Manuscript

NIH-PA Author Manuscript

induce OPC proliferation and oligodendrogenesis outside of lesions but prevent it inside lesions are not understood.

After SCI, the time course of OPC proliferation coincides with the evolution and duration of intraspinal hemorrhage. Moreover, the margins of the areas affected by PHN correlate with areas of proliferating and differentiating OPCs. Based on these spatial-temporal dynamics of acute lesion environment and cell proliferation, we hypothesize that vascular disruption and the resultant hemorrhage play a prominent role in stimulating OPC proliferation and differentiation into new oligodendrocytes after SCI.

The extent to which bleeding affects endogenous OPCs after SCI has not been examined, mostly because it is difficult to separate the effects of blood from those caused by mechanical injury after traumatic SCI. Therefore, to study the effect of hemorrhage on OPCs *in vivo*, a reproducible model was needed that mimicked post-SCI hemorrhage without the shear stress and axonal stretching caused by mechanical impact (Blight and Decrescito, 1986). To date, no intraspinal bleeding models have been characterized, but rodent models of intracerebral hemorrhage are widely used. The two most common models of intracerebral hemorrhage are created either by injecting autologous whole blood or collagenase into the brain (Bullock et al., 1984; Rosenberg et al., 1990a; MacLellan et al., 2008; 2010). Although blood injection directly tests the effect of blood-borne molecules on CNS tissue, the blood quickly clots and does not replicate the dynamic process of progressive hemorrhagic necrosis occurring after CNS trauma (Griffiths et al., 1978; Simard et al., 2012). In contrast, collagenase digests collagen in the basement membrane of microvessels, causing capillaries to leak and degenerate, thus causing a more gradual progression of hemorrhage (Rosenberg et al., 1990b; MacLellan et al., 2008). In this way the collagenase model is more similar to traumatic vascular damage than the whole blood injection model (Rosenberg et al., 1990b; MacLellan et al., 2008; 2010).

By adapting this model to the spinal cord, the acute SCI microenvironment was replicated in the absence of the biomechanical forces that occur during mechanical injury. This model was characterized and compared with a standardized model of spinal contusion injury, including examining macrophage distribution, iron accumulation, and changes in oligodendrocyte lineage cells. The expression and distribution of ERK1/2 and STAT3, factors activated acutely after traumatic SCI that play a role in glial responses, were also investigated.

The data show that vascular damage and bleeding are sufficient to kill oligodendrocytes and increase OPC proliferation and differentiation into new oligodendrocytes. Also, bleeding activates ERK and STAT3 signaling pathways, and results in iron-laden macrophage accumulation and axon and myelin loss, similar to contusion injuries. Together, these results are an important step in understanding how bleeding, one of the earliest components of secondary injury cascades after SCI, affects endogenous OPC proliferation and oligodendrocyte replacement as well as other cellular responses. A clear understanding of mechanisms initiating spontaneous glial repair is needed to design the most optimal treatments for SCI and other conditions in which oligodendrocytes are lost. This model will provide a great starting point for those types of studies.

NIH-PA Author Manuscript
NIH-PA Author Manuscript
NIH-PA Author Manuscript

Materials and Methods

Spinal Cord Injuries

All procedures conformed to NIH and The Ohio State University Institutional Animal Care and Use Committee guidelines. Adult female Sprague-Dawley rats (230-250 g) were anesthetized with ketamine (80mg/kg i.p.) and xylazine (10mg/kg i.p.). Using aseptic technique, the skin was cleaned and the spinal cord was exposed via a laminectomy at the T8 vertebral level and the animal secured in a stereotactic frame using modified beveled forceps attached to the T7 and T9 dorsal processes. Groups and group sizes are outlined in Table 1.

Intraspinal hemorrhage (ISH)

Pilot studies were conducted to determine the ideal volume and concentration of collagenase (type VII, Sigma-Aldrich, St. Louis, MO) that would create reproducible intraspinal hemorrhage. After testing ranges from 0.02–0.2 U/0.5μL collagenase, it was determined that 0.5μL of 0.04U collagenase was ideal and was used for all subsequent experiments (n=83). For these, a beveled glass pipette with a 30-40μm tip was positioned 0.7mm lateral to the midline and inserted 0.9mm ventral to the surface of the spinal cord. A pneumatic picopump microinjection device (DKI, Tujunga, CA) was used to inject 0.5μL of vehicle (sterile 0.9% saline) or 0.04U collagenase using three ~167nl boluses over a total of 2 min. To prevent backflow, the pipette remained in place for 3 min after the final bolus and then was raised half of the distance to the spinal cord surface. After another 1 min pause, the pipette was completely removed. The location of the microinjection was marked on the cord surface with charcoal (Sigma-Aldrich). Rats received BrdU at different post-injury intervals and were perfused between 1 – 28dpi. See Table 1 for details.

Nine animals were excluded from the study due to improper location or complete lack of lesion formation, likely due to problems such as clogged pipettes during the microinjections (excluded from Table 1). The collagenase solution had an EU value of 0.161EU/mL according to the LAL endotoxin test (Cell Sciences; Canton, MA) indicating it was not a significant source of endotoxin.

Lateral Hemi-contusion

A laminectomy was performed at T8 as above (n=16). The same stereotactic frame was secured under the tip of an Infinite Horizons SCI device (Precision Systems and Instrumentation, Lexington, KY) and a 1 mm diameter impact probe was positioned approximately 0.2mm lateral to the midline. The probe was lowered and the lesion site flooded with saline up to the tip of the probe. The force was set to 200 kDynes and the computer controlled probe was rapidly driven into then removed from the spinal cord. The recorded actual forces were between 205 – 384 kDynes (average 299, SD 51.6). Displacements ranged between 846 – 1446 mm (average 1199), SD 180). Rats were injected with BrdU and sacrificed between 1 – 28dpi. See Table 1 for details.

NIH-PA Author Manuscript

NIH-PA Author Manuscript

NIH-PA Author Manuscript

Post-operative Care

Muscles were sutured with vicryl and the incision closed with wound-clips. Animals were given 5cc saline subcutaneously, and their cages placed on slide warmers overnight. Manual bladder expression was performed daily until spontaneous bladder control was regained, which was typically by 3dpi in both injury types.

Bromo-deoxyuridine Injections

Bromo-deoxyuridine (BrdU; Roche Diagnostics, Indianapolis, IN) was injected once daily (i.p. 20mg/ml, 50mg/kg). Animals in each survival group received a specific BrdU pulsing regimen as outlined in Figure 1 and Table 1.

Tissue Processing

Rats were transcardially perfused with heparinized PBS (2U/mL) until the blood was cleared, followed by 4% paraformaldehyde (PFA) pH 7.4 for 10 min at a speed of ~30mL/min. Spinal cords were dissected and post-fixed in PFA for 2h, then placed in 0.2M phosphate buffer overnight. The cords were then transferred to a 30% sucrose solution for 2–3 days. Intraspinal hemorrhage spinal cords were blocked into 1.5 cm pieces centered on the microinjection site, while hemi-contusion cords were blocked into 0.8 cm pieces. The tissue was embedded in OCT compound (Sakura Finetek, Torrance, CA) and frozen on dry ice. Tissue blocks were stored at - 80°C until they were cut on a cryostat into 10μm transverse sections at a rostral to caudal orientation and collected sequentially on positively charged glass slides.

Immunohistochemistry

Immunohistochemistry for light microscopy was performed as previously described (Schonberg et al., 2007). Briefly, sections were rinsed with 0.1M PBS, and non-specific antigen binding was blocked using 4% bovine serum albumin/0.1% Triton X-100/PBS. For NG2 staining, 0.3% Triton-X-100 was used instead of 0.1%, and slides were incubated with primary antibody for 18h at RT. All other primary antibody incubations were overnight at 4°C. Antibodies included the following: rabbit anti-NG2 (1:400; US Biological, Swampscott, MA); mouse CC1 (antibody clone for oligodendrocytes, also called anti-APC, 1:800 Abcam, Cambridge, MA); mouse anti-CD11b for microglia and macrophages (1:2000, Ox42 clone; Serotec, Raleigh, NC); mouse anti-glial fibrillary acidic protein for astrocytes (1:4000; Sigma-Aldrich); mouse anti-BrdU (1:200 G3G4; Developmental Studies Hybridoma Bank, Iowa City, IA); rabbit anti-pSTAT3 (1:200; Cell Signaling, Danvers, MA) and mouse anti-neurofilament for axons (1:2000; Developmental Studies Hybridoma Bank (DSHB)). To visualize myelin and axons, neurofilament (NF) labeling (1:2000, RT97 clone, DSHB) was combined with Eriochrome Cyanine (EC) staining, as described before (Schonberg et al., 2007). Ki67 (1:200, MIB-5 clone, Dako, Carpinteria, CA) immunolabeling was preceded by high pH antigen retrieval, and incubated for 2h at RT.

Fluorescent immunohistochemistry was also performed as described previously (Schonberg et al., 2007; Tripathi and McTigue, 2008). Primary antibodies were: mouse collagen IV (1:1000 DSHB), mouse CC1 (1:2500); biotinylated sheep anti-BrdU (1:250, Abcam); mouse anti-NG2 (1:200 US Biological, Swampscott, MA) and rabbit anti-pERK1/2 (1:100; Cell

NIH-PA Author Manuscript

NIH-PA Author Manuscript

NIH-PA Author Manuscript

Signaling, Danvers, MA). 4% bovine serum albumin/0.1% Triton X-100/PBS blocking solution was used for the CC1/BrdU and collagen IV immunohistochemistry; all other antibodies used blocking solution with 0.3% Triton-X. Secondary antibodies were Alexa-Fluor 488 (1:500) and Alexa-Fluor 546 (1:1000) (Invitrogen). Fluorescent images were generated using an Olympus FV 1000 Confocal system at the Campus Microscopy and Imaging Facility, The Ohio State University. Proper controls were performed to ensure specificity of all immunolabeling.

Histology

Endogenous peroxidase activity was used to visualize red blood cells through reaction with diaminobenzidine (DAB) (Vector, Burlingame, CA) without prior treatment with hydrogen peroxide or ABC solution. Ferric iron was visualized using Perls Iron stain as described previously (Schonberg and McTigue, 2009; Sauerbeck et al., 2013).

Tissue Analysis

Lesion Area—Sections stained with EC and NF were used to define the lesion and peri-lesion areas. Digitized images of EC/NF labeled cross-sections were captured using MCID image analysis software (InterFocus Imaging, Cambridge, England). The lesion area, defined as lack of intact myelin or axon immunoreactivity, was digitally outlined and its target area was measured. Lesion size was expressed as proportional area, which is calculated as target area of lesion divided by total cross-sectional area and expressed as a percentage. All figures show lesions that are representative of the mean for each time point.

3D Reconstruction—A representative animal was chosen for 3D visualization of the lesion site from the ISH and hemi-contusion groups based on the mean percent lesion area of epicenter and length of lesion. EC/NF stained cross-sections spanning the full rostral-caudal extent of the lesions were digitized via MCID software. Within the 3D Analysis mode of the MCID software, the distance between each cross-section was inputted, and components of each cross-section were manually traced and defined. Automatic 3D rendering was done based on manually defined cross-section parameters.

Red Blood Cell Area Quantification—Images stained for endogenous peroxidase activity were digitized, and the cross-sections were outlined. A threshold was set to capture the area of positive endogenous peroxide staining in each cross-section, and the proportional area of positive staining was measured.

Cell Quantification—Labeled cell profiles were manually counted in the ipsilateral side of transverse cross-sections by focusing through the tissue at 40x by an investigator blinded to the time point or lesion type. Sampling was done with the aid of a counting reticle. Cell profiles were considered NG2+ cells if they contained a nucleus (identified with neutral red or BrdU) surrounded by a well-circumscribed NG2+ cell body surrounding > 75% of the nuclear diameter in the same plane of focus. Cells determined to be NG2+ pericytes or macrophages were excluded from counts based on morphology (Tripathi and McTigue, 2007). Briefly, the NG2 membrane label was separated from the nucleus by a large amount of cytoplasm in macrophages, and pericytes displayed a crescent shape and were associated

NIH-PA Author Manuscript

NIH-PA Author Manuscript

NIH-PA Author Manuscript

with blood vessels. NG2 cells identified in this way are termed “oligodendrocyte progenitor cells” or “OPCs” throughout the manuscript.

In sections immunolabeled for CC1/BrdU, a counting frame of 0.05mm^2 size was used to systematically collect images along the lesion borders using an Olympus FV 1000 Confocal microscope. The first counting frame was positioned randomly along the border, and then sampling proceeded circumferentially around the lesion, leaving one counting frame area between each sampled region to avoid double-counting cells. CC1+ and CC1+/BrdU+ cells were manually quantified using Fluoview Viewer Software (Olympus); samples within the white matter and gray matter lesion borders within each cross-section were averaged. For all cell counts, data were collected as cells/mm^2 based on the area of the ipsilateral cross-section (for NG2 and NG2/BrdU cells) or the counting frame area (CC1 and CC1/BrdU). Data were converted to cells/volume (mm^3) by dividing area data by the section thickness (0.01mm).

Protein Isolation

Animals received vehicle or collagenase microinjection as described above. At 1 or 7 days post- microinjection (n=3/group), animals were perfused with physiological saline to clear intravascular blood. A 4mm block of fresh spinal cord centered on the microinjection site was dissected and placed into RIPA buffer. Halt protease and phosphatase inhibitors (Thermo Scientific) and EDTA were added, and the samples homogenized. Homogenates were centrifuged at 4°C for 10 min at 10,000 g and the supernatant aliquoted and stored at −80°C.

Western Blots

Protein samples were thawed and the concentrations determined by BCA assay. 30μg protein/sample was prepared in 1X LDS NuPAGE sample buffer and 1X NuPAGE Reducing agent. Samples were heated at 95°C for 10 min and then run on a 4–12% Bis-Tris NuPAGE gel (Invitrogen) at 200V until the sample dye reached the foot of the gel (40–55min.). Proteins were transferred to a nitrocellulose membrane at 30V for 1.5h and then blocked for 1h using 5% BSA in wash buffer (0.5% Tween in 0.1M PBS). Primary antibodies were incubated in 5% BSA at 4°C overnight with shaking. Membranes were washed and incubated with the appropriate HRP-conjugated secondary antibodies at RT for 1h. The Super Signal West Pico kit (Thermo Scientific) was used to chemiluminescently image the bands on a Kodak imager (Carestream Health Inc. Rochester, NY). The Precision Plus Protein WesternC Standard (Biorad, Hercules, CA) ladder was used to determine protein size. In order to re-probe the membranes with total ERK, membranes were stripped of their antibodies using the Restore Western Blot Membrane Stripping Buffer (Thermo Scientific).

Statistics

Graphpad Prism software 5.0c (San Diego, CA) was used for statistical analysis and constructing graphs. Differences between multiple groups were analyzed using one-way ANOVA followed by a post-hoc test of multiple comparisons. For lesion area, DAB area, and western blot analyses, Bonferroni’s post-hoc test was used. In NG2 cell and total

NIH-PA Author Manuscript

NIH-PA Author Manuscript

NIH-PA Author Manuscript

oligodendrocyte analyses, a Dunnett's post-hoc analysis was used to compare injury groups to controls. For comparison of ISH time points to their respective hemi-contusion time points, Bonferroni's post-hoc test was used. CC1/BrdU data were analyzed with a Two-way ANOVA comparing location and time, followed by Bonferroni's post-hoc test. In all analyses, the 1d and 7d vehicle groups were not significantly different from each other, and were therefore combined as a single "vehicle" group.

Results

Unilateral collagenase-induced intraspinal hemorrhage induces well-defined lesions and mild locomotor deficits

Spinal cords collected 1h after collagenase microinjection had no outward sign of hemorrhage, while hemorrhage was clearly visible by 4h post-microinjection (Fig. 2A,B). Staining cross- sections with DAB for endogenous peroxidase activity, which mainly denotes red blood cells and neutrophils, confirmed these observations. There was a small area of DAB reactivity in 3 out of 5 animals at 1h, while all spinal cords from the 4h group had a large area of hemorrhage (Fig. 2C,D). Accordingly, collagen IV immunohistochemistry revealed that microvasculature was intact at 1h, while collagen IV-labeled vessels were completely absent in the area of DAB reactivity by 4h, confirming the destruction of collagen and microvessels by collagenase (Fig. 2E,F).

At 1 and 3d post-ISH, blood was still visible grossly in the spinal cords, and the rostral-caudal length of hemorrhage was consistent across animals (Fig. 2G). Hemorrhage was not visible externally after 3d or in vehicle control spinal cords at any time. Quantification of the area of DAB after ISH revealed peak levels at 4h – 1d post-ISH, which declined thereafter (Fig. 2H).

Our laboratory has detected differences in gray and white matter cellular and growth factor responses after SCI (Tripathi and McTigue, 2007; 2008; Almad and McTigue, 2010). Therefore our goal was to establish hemorrhage-induced lesions with sufficient spared gray and white matter to study differential cellular dynamics at the lesion borders. Thus, collagenase was targeted to the lateral white matter – gray matter border. At 1 and 3d after ISH, prominent lesions containing myelin debris and damaged axons correlated with area of DAB in adjacent sections (Fig. 3A-D). Note that at 1d post-ISH, DAB was also present outside the lesion, suggesting leakage of vascular contents beyond the area of vessel loss (Fig. 3A). By 7d post-ISH, DAB staining was confined to hemosiderophages scattered throughout regions previously occupied by blood (Fig. 3E). At this time, most debris had been cleared and lesions were mostly devoid of myelin and axons (Fig. 3F).

To compare cellular responses between mid-thoracic ISH and contusion injury, which includes hemorrhage and all other components of secondary injury, we developed a unilateral thoracic hemi-contusion model. First, locomotor recovery was compared in ISH and hemi-contusion rats using the BBB open field locomotor rating scale (Basso et al., 1995). Vehicle microinjection (saline) caused no behavioral deficits at any time. By 4h after collagenase injection, visual inspection of animals revealed obvious locomotor deficits. A formal BBB test was not performed, however, due to concern that some animals had not

NIH-PA Author Manuscript

NIH-PA Author Manuscript

NIH-PA Author Manuscript

completely recovered from anesthesia. At 1d after collagenase microinjection, rats had mild locomotor deficits on the ipsilateral hindlimb including occasional missed steps, poor toe clearance, rotated paw position, and trunk instability (mean BBB score of 15, n=22; Fig. 4B). These deficits declined by 3d, at which time BBB scores were ~19, which then plateaued ~20 by day 21 due to persistent trunk instability (Fig. 4B).

In comparison, hindlimb deficits were more severe in hemi-contusion animals at 1dpi (mean ipsilateral score of 10, n=16; Fig. 4B). Half of the animals also had deficits in contralateral stepping. Animals recovered consistent stepping and forelimb-hindlimb coordination by 5dpi (mean BBB score of 18.3, n= 5), which was maintained through 28dpi. Deficits in ipsilateral toe clearance and paw placement were maintained in 4/5 animals and all had trunk instability at 28dpi. Thus, the two lesion paradigms produced mild and mostly transient locomotor deficits (Fig. 4B).

Next, lesion size and distribution were compared in the two injury models. Hemi-contusion lesion epicenters occupied a greater cross-sectional area than ISH lesions. Along the rostral-caudal extent, ISH lesions maintained a relatively stable diameter, whereas hemi-contusion lesions had a fusiform shape (similar to midline contusions) (Fig. 4A). On average, ISH lesions were >2-times longer than hemi-contusion lesions (Fig. 4C,D). These differences are most likely due to the localized spread of collagenase along longitudinal white matter tracts whereas contusion damage spreads radially within a spinal segment due to PHN, then longitudinally as a result of stretching and sheer force on axons and vasculature (Blight and Decrescito, 1986; Blight, 1988; Tator and Koyanagi, 1997).

After ISH, mean cross-sectional lesion area decreased significantly between 7d – 28d (Fig. 5A-E), and the total cross-section area declined ~10% by 28dpi (Fig. 5F). Reduced lesion and cross- sectional areas were most likely due to lesion collapse and tissue shrinkage, similar to what occurs after spinal contusion injury (McTigue et al., 2001; 2006; Rabchevsky et al., 2007).

Macrophage activation and iron accumulation after ISH

Iron accumulation and robust macrophage activation are common features of contusion injuries and are thought to occur, at least in part, as a result of intraspinal bleeding and vascular disruption (Popovich et al., 1997; Popovich and Hickey, 2001; Rathore et al., 2008; Sauerbeck et al., 2013). To determine to what extent intraspinal bleeding alone evokes these responses, we examined ISH lesions for macrophage activation and iron accumulation. At 1d post-ISH, microglia were less ramified and more amoeboid within and around lesions compared to controls (Fig. 6A,B). Between 3 - 7d, macrophage accumulation increased in ISH lesions, especially in previous gray matter region (Fig. 6C). In contrast, macrophages were more evenly distributed throughout former gray and white matter in hemi-contusion lesions at 7d (Fig. 6D).

Iron accumulation and increased expression of ferritin, the main iron storage protein, occur after spinal contusion injury and are thought to result from red blood cell breakdown subsequent to intraspinal bleeding. Further, iron and ferritin both affect oligodendrocyte lineage cell responses (Zhang et al., 2006; Schonberg and McTigue, 2009; Todorich et al.,

NIH-PA Author Manuscript

NIH-PA Author Manuscript

NIH-PA Author Manuscript

2009; Schonberg et al., 2012). Therefore, iron deposition and ferritin expression were compared in ISH and hemi- contusion tissue. Iron was first noted in lesions at 3d and was prominent by 7d in both models (Fig. 6A-D). As noted before in contusion SCI (Sauerbeck et al., 2013), iron remained high through 28d in both injury models (not shown). Iron distribution closely matched macrophage localization in each model, suggesting macrophages accumulated excess iron. Iron accumulation stimulates cellular ferritin production and, accordingly, ferritin/Cd11b double-labeling revealed robust ferritin expression by macrophages in ISH lesions (Fig. 6E-G), thus confirming that macrophages accumulate iron after ISH. These results reveal that intraspinal bleeding is sufficient to induce robust macrophage activation, iron accumulation and ferritin expression.

ISH stimulates oligodendrocyte progenitor cell proliferation and accumulation

Robust NG2+ OPC proliferation occurs acutely after spinal contusion injury (Zai and Wrathall, 2005; Tripathi and McTigue, 2007). The factors that stimulate this proliferation, however, are unknown. To determine if intraspinal bleeding alone can stimulate OPCs to divide, rats receiving ISH were given BrdU at 4h - 22h post-injection and spinal cords examined at 24h post-ISH (Fig. 1, Table 1). The number of NG2/BrdU+ OPCs increased 2-fold ipsilateral to the lesion by 24h compared to vehicle and naive controls ($p < 0.01$; Fig. 7 A,B,D), revealing that vascular disruption and bleeding, either directly or indirectly, stimulate rapid OPC proliferation.

To determine how early OPCs respond to ISH, a group of animals received BrdU immediately after collagenase microinjection and were sacrificed at 1h, while another group was given BrdU at 1h and were sacrificed at 4h (Table 1). No BrdU positive NG2 cells were present at either 1 or 4h suggesting NG2+ OPCs proliferate after 4h post-ISH. To confirm lack of OPC proliferation at 1h and 4h after ISH, sections were labeled for NG2/Ki67. Contralateral NG2/Ki67 numbers were comparable to historical data from vehicle-injected spinal cords in 3 different studies (unpublished data); therefore contralateral spinal cord hemispheres were used as controls. Quantification of NG2+ OPCs expressing Ki67 confirmed a lack of OPC proliferation at 1 and 4h (Fig. 7C). Total Ki67 also was not different (not shown). Interestingly, there was a trend for reduced OPC proliferation at 4h ($p < 0.0575$), indicating possible toxicity at that time point.

A separate cohort of animals received BrdU for 3d post-ISH and NG2/BrdU cells were quantified at 3d and 7d (see Fig. 1, Table 1). In these spinal cords, NG2/BrdU cell numbers were comparable to the 1d group (Fig. 7D). To determine if OPCs continued to divide after 3d post- ISH, a group of rats was given daily BrdU at 4 – 7 d. These sections also had a 2-fold increase in NG2/BrdU cells at 7d post-ISH ($p < 0.01$; data not shown) revealing that OPCs divide throughout the first week after intraspinal bleeding. Based on changes in oligodendrocytes (see below), the stable levels of NG2/BrdU cells in the face of continued proliferation likely reflect differentiation of some NG2/BrdU cells into oligodendrocytes during this time.

To examine overall OPC cell population dynamics, the total number of NG2+ OPCs was quantified ipsilateral to ISH. At 1d post-ISH, OPC numbers were comparable to naïve levels, despite complete OPCs loss in the area of bleeding (Fig. 7E). This means a higher

NIH-PA Author Manuscript

NIH-PA Author Manuscript

NIH-PA Author Manuscript

density than normal was present in spared tissue, likely due to robust proliferation between 4 – 24h. By 7d post-ISH, OPCs had risen slightly and were present in both spared and lesioned tissue. OPC numbers continued to rise over time such that by 28d after ISH, they were significantly greater than at early times and were ~ 2-fold higher than controls (Fig. 7E). Thus, OPC proliferation increased within 24h after ISH and continued throughout the first week, which resulted in maintenance of normal OPC numbers at 1d and increased numbers over the first month.

Comparison of oligodendrocyte progenitor cell dynamics in ISH versus hemi-contusion

After hemi-contusion injury, NG2/BrdU cells were slightly lower than naïve at 24h but then increased 9-fold by 7dpi ($p < 0.001$ vs. 1dpi; Fig. 7D). Thus, compared to ISH in which NG2/BrdU numbers were stable between 1–7dpi, NG2/BrdU cells started lower then increased significantly over 7dpi. Despite the larger lesions in the hemi-contusion sections, the number of NG2/BrdU cells at 7dpi was not significantly different from that in 7dpi ISH tissues (p=0.08).

In contrast to ISH, total OPC numbers were slightly lower than control 1d after hemi-contusion. By 7d post-injury, OPC numbers had increased >3-fold and were present in spared and lesioned tissue. At this time, OPCs were significantly higher than 1dpi and naive tissue (Fig. 7E), which is consistent with the robust OPC proliferation during this time (Fig. 7D). OPC number decreased slightly by 28dpi. Overall, OPC numbers at 1d, 7d, and 28dpi were not significantly different between ISH and hemi-contusion lesions.

Oligodendrocyte genesis replaces oligodendrocytes lost after ISH

Several studies have documented loss oligodendrocytes by 24h followed by replacement with new cells after spinal contusion (McTigue et al., 2001; Zai and Wrathall, 2005; Rabchevsky et al., 2007; Tripathi and McTigue, 2007). Therefore, we investigated whether ISH also stimulated oligodendrogenesis. Oligodendrocytes were reduced 20% at 4h and 50% by 1d after ISH ($p < 0.001$). Thus, vascular damage and bleeding into the spinal cord caused rapid oligodendrocyte loss (Fig. 8D). Notably, oligodendrocytes were lost in the lesions as well as in spared tissue, indicating that toxic molecules from the primary lesion negatively affected nearby spared tissue; this is consistent with the peroxidase staining outside the lesion at 1d post-ISH (see Fig. 3B). Oligodendrocyte numbers rose slightly by 3dpi, then increased further to control levels by 7d post-ISH (Fig. 8A-D). Very few oligodendrocytes were in the lesions after 1dpi and, as noted previously after contusion injury, oligodendrocyte density along lesion borders was greater than naïve levels by 7d post-ISH suggesting a robust oligogenic response in this region (Fig. 8A-C).

Oligodendrocyte numbers again dropped slightly but significantly by 14dpi (Fig. 8D), but then recovered to control levels by 28dpi (Fig. 8D). This delayed loss may reflect chronic apoptosis as shown in contusion and intracerebral hemorrhage models (Crowe et al., 1997; Warden et al., 2001; Prunell et al., 2005) and suggests oligodendrocyte generation may continue for weeks after ISH.

NIH-PA Author Manuscript

NIH-PA Author Manuscript

NIH-PA Author Manuscript

To confirm that the increase in oligodendrocytes was due to differentiation of OPCs dividing early after ISH, sections were examined for BrdU+ oligodendrocytes 7d after ISH in rats given BrdU on 1–3dpi. BrdU+ oligodendrocytes were significantly increased by 7d after ISH, especially in the gray matter lesion border (Fig. 8E). This means OPCs proliferating in the first 3 days after ISH differentiated into new oligodendrocytes by 7d. When animals given BrdU throughout the first 7d survived to 14d and 28d after ISH, the number of BrdU+ oligodendrocytes remained constant in the gray matter (Fig. 8E). In white matter, however, BrdU+ oligodendrocyte numbers rose >4-fold between 14 - 28d post-ISH to reach a significantly higher level than controls ($p < 0.05$; Fig. 8E). Thus, oligodendrocyte generation from progenitors dividing during week one continues for several weeks after ISH.

Next, oligodendrocyte number after ISH were compared to hemi-contusion. There were fewer oligodendrocytes ipsilateral to hemi-contusion at 1d – 28d post-injury (Fig. 8D), likely due to the cell loss in the larger contusion lesions. However, similar to ISH and mid-line thoracic contusions, overall oligodendrocyte numbers increased significantly over time likely due OPC differentiation (Fig. 8D). Thus, intraspinal bleeding and contusion both induce acute oligodendrocyte loss and subsequent replacement by new cells.

Oligodendrocyte to OPC ratio

To get an idea of the relationship between changes in oligodendrocyte and OPC numbers after ISH and contusion, we calculated the ratio of oligodendrocytes to OPCs at 1, 7 and 28d post- injury (Table 2). Sections from uninjured spinal cords had an oligodendrocyte/OPC ratio of 10.7, meaning that there are ~10 oligodendrocytes for every 1 NG2+ OPC in control tissue. After ISH, this ratio declined to 5 oligodendrocytes/OPC at 1d, and declined further to ~4 oligodendrocytes/OPC at 28d post-ISH due to the greater expansion of the OPC population.

Ipsilateral contusion tissue had a lower oligodendrocyte/OPC ratio of ~1.5 at 1dpi, mainly due to greater oligodendrocyte loss. However, similar to ISH, the ratio increased to 4 oligodendrocytes/OPC by 28d post-injury, again mostly due to a greater increase in OPCs compared to oligodendrocytes. Thus, the shift in the balance of oligodendrocytes to OPCs is comparable after ISH and hemi-contusion.

pERK1/2 and pSTAT3 increase acutely after ISH

To examine possible signaling mechanisms involved in glial responses to ISH, protein from 1d and 7d post-ISH tissue was probed for pERK1/2, intracellular kinases involved in OPC responses and known to increase after acute SCI (Frost et al., 2008; Hu et al., 2008; Yu et al., 2010; Guardiola-Diaz et al., 2011). At 1d post-ISH, pERK1/2 protein was ~10-fold higher compared to control, revealing an acute robust activation of the MAPK pathway (Fig. 9A,B). By 7dpi, pERK1/2 had returned to basal levels (Fig. 9A,B).

pSTAT3 regulates proliferation, differentiation and survival, and is upregulated by OPCs following spinal contusion injury (Tripathi and McTigue, 2008). At 1d after vehicle injection, a low level of pSTAT3 was detected, indicating that STAT3 is activated by mild intraspinal stimuli such as a laminectomy and saline microinjection (Fig. 10A,B). After ISH,

NIH-PA Author Manuscript

NIH-PA Author Manuscript

NIH-PA Author Manuscript

however, pSTAT3 expression was 9-fold higher than controls, revealing that intraspinal bleeding potently activates STAT3 (Fig. 10A,B). By 7dpi, pSTAT3 levels declined toward baseline (Fig. 10A,B). Immunohistochemistry revealed few STAT3+ profiles in naïve or vehicle injected tissue. In contrast, 1d post-ISH sections contained abundant pSTAT3+ nuclei throughout the ipsilateral cross-sections. At this time, about ~18% of OPCs were immunoreactive for pSTAT3 (in contrast to zero in controls). The majority of pSTAT3 expressing cells at 1dpi were astrocytes, with some oligodendrocytes also co-labeled (Fig. 10C). At 3 and 7dpi, pSTAT3 was almost exclusively expressed by reactive astrocytes along the lesion border. Thus, STAT3 is robustly activated acutely after ISH and may comprise part of the signaling cascades driving the post-ISH OPC (and astrocyte) response.

Discussion

ISH model development

Despite the SCI pathology that kills mature oligodendrocytes, the tissue environment around the lesion favors NG2+ OPC cell proliferation and differentiation (McTigue et al., 2001; Zai and Wrathall, 2005; Rabchevsky et al., 2007; Tripathi and McTigue, 2007; Sellers et al., 2009; Powers et al., 2013). The many cellular cascades initiated by traumatic SCI, however, complicate identifying factors that initiate this response. A useful strategy to examine triggers of cell responses is to study specific aspects of SCI in isolation. For instance, in previous work, we examined the effect of intraspinal macrophage activation and ferritin expression on OPCs in the adult spinal cord and showed that macrophages activated by TLR-4 stimulate migration and expansion of this population (Schonberg et al., 2007; 2012). In the current study, the glial responses to intraspinal bleeding were examined, since hemorrhage is one of the first events after trauma and a major initiator of secondary cellular reactions (Mautes et al., 2000; Simard et al., 2010; Popovich et al., 2011).

Although a long-held assumption, these results provide the first direct evidence that vessel disruption and intraspinal bleeding alone initiate many aspects of traumatic SCI pathology, including rapid axon and myelin loss, macrophage and iron accumulation, and cell death. This is in line with pre-clinical studies showing that ameliorating post-SCI vascular damage and hemorrhage improves anatomical and functional outcome (Simard et al., 2007; Han et al., 2010; Herrera et al., 2010; Benton and Hagg, 2011). Thus, the ISH model is a useful tool for investigating secondary injury mechanisms and cellular responses to SCI. In addition, it reveals how acute events shape chronic post-injury cell responses.

Most previous studies examining glial responses to SCI have used midline contusions or dorsal hemisections. To account for the differing location and milder unilateral ISH injury, glial responses to ISH were compared with those after moderate unilateral contusion (hemi-contusion). The different rostral-caudal distribution of the lesions between the two models, and the more defined borders (i.e. less diffuse nature) of ISH lesions illustrate how injury biomechanics alter lesion morphology (Maikos and Shreiber, 2007; Choo et al., 2009; Pleasant et al., 2011). Blight and Decrescito (1986) demonstrated the importance of spinal cord displacement in determining stretch and sheering forces, and that a dorsal impact distributes these forces unevenly in the tissue. Given that studies using a unilateral cervical SCI model revealed localized ipsilateral bleeding within hours that spread throughout the

NIH-PA Author Manuscript

NIH-PA Author Manuscript

NIH-PA Author Manuscript

tissue by 24h (Popovich et al., 2011; Simard et al., 2012), it is not surprising that a much more “contained” focal transverse lesion is obtained in ISH in the absence of stretch and sheering forces.

In this study, epicenters were compared between the two models despite different lesion sizes because the effect of primary injury in hemi-contusion would be greatest at the impact site and would therefore give a more accurate comparison between mechanical and purely vascular injuries. Some implications of this paradigm are discussed below.

OPC proliferation after ISH and hemi-contusion

Compared to naïve tissue, NG2/BrdU cells were 200% higher 1d post-ISH, in contrast to hemi- contusion tissue in which they were 50% lower. An obvious explanation would be that the larger lesions in hemi-contusion caused greater OPC loss. To evaluate if this may contribute to the differences, we quantified NG2/BrdU+ OPCs at distal locations where cross-sectional lesion areas were more similar between ISH and hemi-contusion (not shown). Both ISH and hemi- contusion tissue had greater OPC proliferation compared to epicenter and there was no significant difference between the groups. Thus, it is likely (and reasonable) that the amount of spared tissue plays a role in determining how many progenitors divide early after injury. By extension, however, it would be predicted that OPC proliferation also would be increased contralateral to the hemi-contusion. However, contralateral NG2/BrdU cell number was not different from naïve at 24h (data not shown). Thus, the tissue environment surrounding hemorrhage promotes acute OPC proliferation while the combination of hemorrhage plus mechanical injury, at least at the epicenter, does not.

Since bleeding peaked by 4h but OPC proliferation had not yet been stimulated, it is unlikely that blood-derived components directly induced OPC proliferation. Significant oligodendrocyte loss had occurred by 4h after ISH. Since OPC proliferation increased subsequent to this oligodendrocyte loss, it is possible that one trigger for acute OPC proliferation was reduced oligodendrocyte numbers after ISH.

Based on total ipsilateral OPC numbers, ~5% of surviving OPCs divided in the first 24h post- contusion while ~17% divided after ISH. One explanation for this difference is the unique oxidative microenvironment created by spinal contusion may prevent maximal proliferation. For example,Sun et al. (2010) showed that RNA oxidation is significantly increased in oligodendrocytes near contusion injuries within 1h but oxidation was not present around pure axon degeneration injuries. In our study, contusion tissue supported later OPC division since NG2/BrdU cells increased 9-fold between 1 – 7dpi. Thus, despite larger lesions and fewer OPCs dividing initially after hemi-contusion, robust OPC proliferation occurred by 7d post-injury. Collectively, this suggests that both models result in robust OPC proliferation during the first week post-injury but that the timing may be somewhat delayed after contusion.

Despite a lesion area virtually devoid of NG2+ OPCs, total OPC numbers ipsilateral to ISH were at pre-injury levels by 1dpi. A rapid response of OPCs after injury would be expected if this cell population has a strong drive to maintain normal cell numbers as suggested by

NIH-PA Author Manuscript

NIH-PA Author Manuscript

NIH-PA Author Manuscript

recent work (Hughes et al., 2013). The presence of the same cell number in a smaller area, however, suggests that the cells responded to factors beyond homeostatic replacement of neighboring cells. These may include blood constituents such as thrombin and platelets diffusing into spared tissue since injecting blood or platelets into the intact CNS increases NG2 reactivity (Rhodes et al., 2006).

Interestingly, OPC numbers continued to rise over time and were 2-fold higher than normal by 28d post-ISH, which suggests continued proliferation and/or enhanced migration. A low number of NG2/Ki67+ cells were present in sections at 14d and 28d post-ISH (not shown), which supports the idea that these cells continued to divide for at least 28d. After hemi-contusion, robust proliferation resulted in a 3-fold increase in total OPCs by 7dpi. OPC numbers declined slightly thereafter, which may reflect differences in the chronic lesion environments and/or ongoing changes in oligodendrocyte numbers as discussed below.

Changes in oligodendrocyte numbers after ISH and contusion

Intraspinal hemorrhage caused a 50% loss of ipsilateral oligodendrocytes by 1dpi, which is consistent with the idea that blood is highly toxic to CNS tissue (Noble and Wrathall, 1989a; Kurland et al., 2012). Oligodendrocyte loss was not restricted to the lesion, suggesting that toxic molecules diffused from lesions into spared tissue, or that the loss of these cells was secondary to the acute effects of the hemorrhage. The observation of endogenous peroxidase staining outside lesion borders suggests the area of blood-brain barrier leakage extended beyond the lesion, which is consistent with historical SCI studies and may be a potential underlying mechanism for effects in spared tissue (Noble and Wrathall, 1989b; Popovich et al., 1996).

Between 1d – 7d post-ISH, total ipsilateral oligodendrocyte numbers returned to basal levels and the density of oligodendrocytes in spared tissue was greater than in naïve spinal cords, as seen previously after SCI (Tripathi and McTigue, 2007). This increased cell density is likely due to differentiation of dividing progenitor cells into oligodendrocytes over the first week. This was verified by the increased BrdU+ oligodendrocytes at 7dpi, most notably in gray matter bordering the injury. The approximate doubling of oligodendrocytes over the first week after ISH may explain why overall NG2+ OPCs and NG2/BrdU cell numbers remained fairly constant after ISH despite ongoing proliferation. That is, a subset of OPCs differentiated into oligodendrocytes by 7dpi, which likely kept the overall cell numbers stable.

In contrast to OPCs, which increased between 7d –14d post-ISH, there was a modest but significant drop in oligodendrocytes during this time, which was mirrored by a >2-fold reduction in BrdU+ oligodendrocytes in white matter. This corresponds to the timing of delayed oligodendrocyte apoptosis and RNA oxidation in oligodendrocytes after SCI (Crowe et al., 1997; Warden et al., 2001; Sun et al., 2010), suggesting that similar pathological mechanisms may occur chronically after ISH. During the subsequent two weeks, BrdU+ oligodendrocytes in white matter increased 4-fold and total oligodendrocyte numbers again returned to naïve levels. Given the continual rise in OPCs and the late rebound in oligodendrocyte numbers, it is clear that while the acute post-ISH environment is toxic to mature oligodendrocytes, it is conducive to proliferation of surviving OPCs,

NIH-PA Author Manuscript

NIH-PA Author Manuscript

NIH-PA Author Manuscript

followed later by differentiation into oligodendrocytes at a high density in the same region these cells were originally lost. Intriguingly, despite a restoration of oligodendrocyte levels after ISH, OPCs continued to accumulate between 14 – 28d, indicating that oligodendrocyte numbers are not the sole regulator of OPC responses.

More robust oligodendrocyte formation at the gray matter lesion borders compared to white matter is consistent with previous work by our lab in spinal contusion showing more pronounced oligodendrocyte genesis at the gray matter lesion borders, and therefore possibly a true difference between the gray and white matter tissue compartments (Tripathi and McTigue, 2007). Consistent with other SCI models, oligodendrogenesis did not occur within collagenase- induced lesions (McTigue et al., 2006). The conformity of these observations in a model of vascular disruption and acute spinal contusion confirms that vascular disruption and the resultant acute tissue environment play a role in forming a lesion that is restrictive to oligodendrogenesis.

Despite a 90% loss by 24h, oligodendrocyte numbers rose to 62% of naïve after hemi-contusion, indicating that robust oligodendrocyte replacement occurred around the lesions. Notably, in both injury models, OPCs increased within the lesions over the first week, but as discussed above, these cells did not differentiate into new oligodendrocytes. Therefore, although hemi-contusion tissue had roughly similar numbers of OPCs at 7d and 28dpi, a greater proportion the OPCs were in the larger lesions where they did not differentiate, which would explain the lower oligodendrocyte numbers in chronic hemi-contusion tissue. It is interesting that despite these differences, the ratio of oligodendrocytes to OPCs in both models plateaued at a similar level.

Potential roles of ERK1/2 and STAT3 in glial responses to ISH

To investigate signaling molecules that may regulate OPCs after ISH, pERK1/2 and pSTAT3 expression were evaluated since they are present acutely after spinal contusion and are potential mediators of OPC responses (Tripathi and McTigue, 2008; Yu et al., 2010; Ishii et al., 2013). Both were increased by 1dpi, suggesting they are rapidly activated by blood-related factors after injury. However, pERK was rarely expressed by OPCs, indicating it unlikely plays a direct role in acute OPC proliferation. In contrast to pERK1/2, a subset of NG2+ OPCs did express pSTAT3 at 1dpi, which may play a role in their proliferation or survival (Dell'Albani et al., 1998; Butzkueven et al., 2002; 2002; Azari et al., 2006). Potential ligands for activating STAT3 include IL-6, CNTF or LIF, all of which are increased after CNS injury (Pineau and Lacroix, 2007; Tripathi and McTigue, 2008). Interestingly, pSTAT3 positive cells were also abundant in the intact contralateral tissue 1d after ISH, signifying widespread injury-related signaling.

Summary

Recent efforts to replicate promising SCI treatments revealed surprising differences in treatment efficacy based on subtle differences in the lesion models (Popovich et al., 2011; Simard and Gerzanich, 2011; Simard et al., 2012). This suggests that there is much still to learn about basic mechanisms underlying the cellular dynamics of injury and endogenous repair mechanisms in the spinal cord. Here, a model of intraspinal bleeding was used to

NIH-PA Author Manuscript

NIH-PA Author Manuscript

NIH-PA Author Manuscript

examine the contribution of hemorrhage to oligodendrocyte lineage cell responses after SCI. We demonstrate for the first time that bleeding alone induces rapid proliferation of NG2+ oligodendrocyte progenitors and a biphasic replacement of oligodendrocytes. In comparison to hemi-contusion, the lesion is spatially restricted and highly toxic to oligodendrocytes. Overall, changes in the patterns of OPC proliferation, oligodendrocyte loss and new oligodendrocyte formation were fairly similar between ISH and hemi-contusion (see Figure 11 for a summary) suggesting that the highly reproducible ISH model provides an important tool for mechanistic studies on early deleterious events after SCI as well as potential treatment options. As is becoming clear, improving outcome after SCI will require combinatorial therapies. Therefore, a more holistic understanding of SCI process is necessary to develop optimal therapies that minimize post-injury damage while preserve or enhance spontaneous reparative responses. Such an understanding is only possible if we have in-depth knowledge of all contributing SCI mechanisms and their interactions with each other.

Acknowledgments

The authors gratefully acknowledge the excellent technical assistance of A. Todd Lash, Andrea Houchin, Evan Goldstein, and Ping Wei. We also thank Dr. Lyn B. Jakeman for her helpful suggestions in experimental design and Drs. Jakeman and Phillip Popovich for critical review of the manuscript. Fluorescent images presented in this report were generated using the Campus Microscopy and Imaging Facility at The Ohio State University. The neurofilament antibody developed by J. Wood, BrdU antibody developed by S.J. Kaufman, and collagen IV antibody developed by H. Furthmayr were obtained from the Developmental Studies Hybridoma Bank developed under the auspices of the NICHD and maintained by The University of Iowa, Department of Biology, Iowa City, IA 52242.This research was supported by NINDS NS059776 and P30-NS045758.

REFERENCES

Almad A, McTigue DM. Chronic expression of PPAR-δ by oligodendrocyte lineage cells in the injured rat spinal cord. J Comp Neurol. 2010; 518:785–799. [PubMed: 20058304]

Azari MF, Profyris C, Karnezis T, Bernard CC, Small DH, Cheema SS, Ozturk E, Hatzinisiriou I, Petratos S. Leukemia inhibitory factor arrests oligodendrocyte death and demyelination in spinal cord injury. J Neuropathol Exp Neurol. 2006; 65:914–929. [PubMed: 16957585]

Basso DM, Beattie MS, Bresnahan JC. A sensitive and reliable locomotor rating scale for open field testing in rats. Journal of Neurotrauma. 1995; 12:1–21. [PubMed: 7783230]

Benton RL, Hagg T. Vascular Pathology as a Potential Therapeutic Target in SCI. Transl Stroke Res. 2011; 2:556–574. [PubMed: 24323683]

Blight A. Mechanical factors in experimental spinal cord injury. J Am Paraplegia Soc. 1988; 11:26–34. [PubMed: 3076595]

Blight AR, Decrescito V. Morphometric analysis of experimental spinal cord injury in the cat: the relation of injury intensity to survival of myelinated axons. NSC. 1986; 19:321–341.

Bullock R, Mendelow AD, Teasdale GM, Graham DI. Intracranial haemorrhage induced at arterial pressure in the rat. Part 1: Description of technique, ICP changes and neuropathological findings. Neurol Res. 1984; 6:184–188. [PubMed: 6152312]

Busch SA, Horn KP, Cuascut FX, Hawthorne AL, Bai L, Miller RH, Silver J. Adult NG2+ Cells Are Permissive to Neurite Outgrowth and Stabilize Sensory Axons during Macrophage-Induced Axonal Dieback after Spinal Cord Injury. Journal of Neuroscience. 2010; 30:255–265. [PubMed: 20053907]

Butzkueven H, Zhang J-G, Soilu-Hanninen M, Hochrein H, Chionh F, Shipham KA, Emery B, Turnley AM, Petratos S, Ernst M, Bartlett PF, Kilpatrick TJ. LIF receptor signaling limits immune-mediated demyelination by enhancing oligodendrocyte survival. Nat Med. 2002; 8:613–619. [PubMed: 12042813]

NIH-PA Author Manuscript

NIH-PA Author Manuscript

NIH-PA Author Manuscript

Choo AM-T, Liu J, Liu Z, Dvorak M, Tetzlaff W, Oxland TR. Modeling spinal cord contusion, dislocation, and distraction: Characterization of vertebral clamps, injury severities, and node of Ranvier deformations. Journal of Neuroscience Methods. 2009; 181:6–17. [PubMed: 19383514]

Crowe MJ, Bresnahan JC, Shuman SL, Masters JN, Beattie MS. Apoptosis and delayed degeneration after spinal cord injury in rats and monkeys. Nat Med. 1997; 3:73–76. [PubMed: 8986744]

Dell'Albani P, Kahn MA, Cole R, Condorelli DF, Giuffrida-Stella AM, de Vellis J. Oligodendroglial survival factors, PDGF-AA and CNTF, activate similar JAK/STAT signaling pathways. J Neurosci Res. 1998; 54:191–205. [PubMed: 9788278]

Frost EE, Zhou Z, Krasnesky K, Armstrong RC. Initiation of Oligodendrocyte Progenitor Cell Migration by a PDGF-A Activated Extracellular Regulated Kinase (ERK) Signaling Pathway. Neurochem Res. 2008; 34:169–181. [PubMed: 18512152]

Gensel JC, Nakamura S, Guan Z, van Rooijen N, Ankeny DP, Popovich PG. Macrophages Promote Axon Regeneration with Concurrent Neurotoxicity. Journal of Neuroscience. 2009; 29:3956–3968. [PubMed: 19321792]

Griffiths IR, Burns N, Crawford AR. Early vascular changes in the spinal grey matter following impact injury. Acta Neuropathol. 1978; 41:33–39. [PubMed: 636835]

Guardiola-Diaz HM, Ishii A, Bansal R. Erk1/2 MAPK and mTOR signaling sequentially regulates progression through distinct stages of oligodendrocyte differentiation. Glia. 2011; 60:476–486. [PubMed: 22144101]

Han S, Arnold SA, Sithu SD, Mahoney ET, Geralds JT, Tran P, Benton RL, Maddie MA, D'Souza SE, Whittemore SR, Hagg T. Rescuing vasculature with intravenous angiopoietin-1 and v 3 integrin peptide is protective after spinal cord injury. Brain. 2010; 133:1026–1042. [PubMed: 20375135]

Herrera JJ, Sundberg LM, Zentilin L, Giacca M, Narayana PA. Sustained Expression of Vascular Endothelial Growth Factor and Angiopoietin-1 Improves Blood-Spinal Cord Barrier Integrity and Functional Recovery after Spinal Cord Injury. Journal of Neurotrauma. 2010; 27:2067–2076. [PubMed: 20799882]

Hill C. Degeneration and Sprouting of Identified Descending Supraspinal Axons after Contusive Spinal Cord Injury in the Rat. Experimental Neurology. 2001; 171:153–169. [PubMed: 11520130]

Horky LL, Galimi F, Gage FH, Horner PJ. Fate of endogenous stem/progenitor cells following spinal cord injury. J Comp Neurol. 2006; 498:525–538. [PubMed: 16874803]

Hu JG, Fu SL, Wang YX, Li Y, Jiang XY, Wang XF, Qiu MS, Lu PH, Xu XM. Platelet-derived growth factor-AA mediates oligodendrocyte lineage differentiation through activation of extracellular signal-regulated kinase signaling pathway. Neuroscience. 2008; 151:138–147. [PubMed: 18093741]

Hughes EG, Kang SH, Fukaya M, Bergles DE. Oligodendrocyte progenitors balance growth with self-repulsion to achieve homeostasis in the adult brain. Nat Neurosci. 2013; 16:668–676. Available at: http://eutils.ncbi.nlm.nih.gov/entrez/eutils/elink.fcgi?dbfrom=pubmed&id=23624515&retmode=ref&cmd=prlinks. [PubMed: 23624515]

Ishii A, Furusho M, Bansal R. Sustained Activation of ERK1/2 MAPK in Oligodendrocytes and Schwann Cells Enhances Myelin Growth and Stimulates Oligodendrocyte Progenitor Expansion. Journal of Neuroscience. 2013; 33:175–186. [PubMed: 23283332]

Juliet PAR, Frost EE, Balasubramaniam J, Del Bigio MR. Toxic effect of blood components on perinatal rat subventricular zone cells and oligodendrocyte precursor cell proliferation, differentiation and migration in culture. Journal of Neurochemistry. 2009; 109:1285–1299. [PubMed: 19476544]

Kigerl KA, Ankeny DP, Garg SK, Wei P, Guan Z, Lai W, McTigue DM, Banerjee R, Popovich PG. System xc^- regulates microglia and macrophage glutamate excitotoxicity in vivo. Experimental Neurology. 2012; 233:333–341. [PubMed: 22079587]

Kurland D, Hong C, Aarabi B, Gerzanich V, Simard JM. Hemorrhagic Progression of a Contusion after Traumatic Brain Injury: A Review. Journal of Neurotrauma. 2012; 29:19–31. [PubMed: 21988198]

MacLellan CL, Silasi G, Auriat AM, Colbourne F. Rodent models of intracerebral hemorrhage. Stroke. 2010; 41:S95–S98. [PubMed: 20876518]

NIH-PA Author Manuscript

NIH-PA Author Manuscript

NIH-PA Author Manuscript

MacLellan CL, Silasi G, Poon CC, Edmundson CL, Buist R, Peeling J, Colbourne F. Intracerebral hemorrhage models in rat: comparing collagenase to blood infusion. Journal of Cerebral Blood Flow & Metabolism. 2008; 28:516–525. [PubMed: 17726491]

Maikos JT, Shreiber DI. Immediate Damage to The Blood-Spinal Cord Barrier Due to Mechanical Trauma. Journal of Neurotrauma. 2007; 24:492–507. [PubMed: 17402855]

Mautes AE, Weinzierl MR, Donovan F, Noble LJ. Vascular events after spinal cord injury: contribution to secondary pathogenesis. Phys Ther. 2000; 80:673–687. [PubMed: 10869130]

McTigue DM, Tripathi R, Wei P. NG2 colocalizes with axons and is expressed by a mixed cell population in spinal cord lesions. J Neuropathol Exp Neurol. 2006; 65:406–420. [PubMed: 16691121]

McTigue DM, Wei P, Stokes BT. Proliferation of NG2-positive cells and altered oligodendrocyte numbers in the contused rat spinal cord. Journal of Neuroscience. 2001; 21:3392–3400. [PubMed: 11331369]

Noble LJ, Wrathall JR. Correlative analyses of lesion development and functional status after graded spinal cord contusive injuries in the rat. Experimental Neurology. 1989a; 103:34–40. [PubMed: 2912748]

Noble LJ, Wrathall JR. Distribution and time course of protein extravasation in the rat spinal cord after contusive injury. Brain Research. 1989b; 482:57–66. [PubMed: 2706482]

Pineau I, Lacroix S. Proinflammatory cytokine synthesis in the injured mouse spinal cord: multiphasic expression pattern and identification of the cell types involved. J Comp Neurol. 2007; 500:267–285. [PubMed: 17111361]

Pleasant JM, Carlson SW, Mao H, Scheff SW, Yang KH, Saatman KE. Rate of Neurodegeneration in the Mouse Controlled Cortical Impact Model Is Influenced by Impactor Tip Shape: Implications for Mechanistic and Therapeutic Studies. Journal of Neurotrauma. 2011; 28:2245–2262. [PubMed: 21341976]

Popovich PG, Guan Z, McGaughy V, Fisher L, Hickey WF, Basso DM. The neuropathological and behavioral consequences of intraspinal microglial/macrophage activation. J Neuropathol Exp Neurol. 2002; 61:623–633. [PubMed: 12125741]

Popovich PG, Hickey WF. Bone marrow chimeric rats reveal the unique distribution of resident and recruited macrophages in the contused rat spinal cord. J Neuropathol Exp Neurol. 2001; 60:676–685. [PubMed: 11444796]

Popovich PG, Horner PJ, Mullin BB, Stokes BT. A quantitative spatial analysis of the blood-spinal cord barrierIPermeability changes after experimental spinal contusion injury. Experimental Neurology. 1996; 142:258–275. [PubMed: 8934558]

Popovich PG, Lemeshow S, Gensel JC, Tovar CA. Independent evaluation of the effects of glibenclamide on reducing progressive hemorrhagic necrosis after cervical spinal cord injury. Experimental Neurology. 2011:1–8.

Popovich PG, Wei P, Stokes BT. Cellular inflammatory response after spinal cord injury in Sprague-Dawley and Lewis rats. J Comp Neurol. 1997; 377:443–464. [PubMed: 8989657]

Powers BE, Sellers DL, Lovelett EA, Cheung W, Aalami SP, Zapertov N, Maris DO, Horner PJ. Remyelination reporter reveals prolonged refinement of spontaneously regenerated myelin. Proc Natl Acad Sci USA. 2013; 110:4075–4080. [PubMed: 23431182]

Prunell GF, Svendgaard N-A, Alkass K, Mathiesen T. Delayed cell death related to acute cerebral blood flow changes following subarachnoid hemorrhage in the rat brain. J Neurosurg. 2005; 102:1046–1054. [PubMed: 16028764]

Psachoulia K, Jamen F, Young KM, Richardson WD. Cell cycle dynamics of NG2 cells in the postnatal and ageing brain. NGB. 2010; 5:57.

Rabchevsky AG, Sullivan PG, Scheff SW. Temporal-spatial dynamics in oligodendrocyte and glial progenitor cell numbers throughout ventrolateral white matter following contusion spinal cord injury. Glia. 2007; 55:831–843. [PubMed: 17390308]

Rathore KI, Kerr BJ, Redensek A, Lopez-Vales R, Jeong SY, Ponka P, David S. Ceruloplasmin protects injured spinal cord from iron-mediated oxidative damage. Journal of Neuroscience. 2008; 28:12736–12747. Available at: http://eutils.ncbi.nlm.nih.gov/entrez/eutils/elink.fcgi?dbfrom=pubmed&id= 19036966&retmode=ref&cmd=prlinks. [PubMed: 19036966]

NIH-PA Author Manuscript

NIH-PA Author Manuscript

NIH-PA Author Manuscript

Rhodes KE, Raivich G, Fawcett JW. The injury response of oligodendrocyte precursor cells is induced by platelets, macrophages and inflammation-associated cytokines. Neuroscience. 2006; 140:87–100. [PubMed: 16631314]

Rosenberg GA, Mun-Bryce S, Wesley M, Kornfeld M. Collagenase-induced intracerebral hemorrhage in rats. Stroke. 1990a; 21:801–807. [PubMed: 2160142]

Rosenberg GA, Mun-Bryce S, Wesley M, Kornfeld M. Collagenase-induced intracerebral hemorrhage in rats. Stroke. 1990b; 21:801–807. [PubMed: 2160142]

Sauerbeck A, Schonberg DL, Laws JL, McTigue DM. Systemic iron chelation results in limited functional and histological recovery after traumatic spinal cord injury in rats. Experimental Neurology. 2013; 248:1–9. [PubMed: 23707216]

Schonberg DL, Goldstein EZ, Sahinkaya FR, Wei P, Popovich PG, McTigue DM. Ferritin Stimulates Oligodendrocyte Genesis in the Adult Spinal Cord and Can Be Transferred from Macrophages to NG2 Cells In Vivo. Journal of Neuroscience. 2012; 32:5374–5384. [PubMed: 22514302]

Schonberg DL, McTigue DM. Iron is essential for oligodendrocyte genesis following intraspinal macrophage activation. Experimental Neurology. 2009; 218:64–74. [PubMed: 19374902]

Schonberg DL, Popovich PG, McTigue DM. Oligodendrocyte generation is differentially influenced by toll-like receptor (TLR) 2 and TLR4-mediated intraspinal macrophage activation. J Neuropathol Exp Neurol. 2007; 66:1124–1135. [PubMed: 18090921]

Sellers DL, Maris DO, Horner PJ. Postinjury Niches Induce Temporal Shifts in Progenitor Fates to Direct Lesion Repair after Spinal Cord Injury. Journal of Neuroscience. 2009; 29:6722–6733. [PubMed: 19458241]

Simard JM, Gerzanich V. When replication teaches more than the original experiment — the saga of the unknown unknown. Experimental Neurology. 2011:1–2.

Simard JM, Popovich PG, Tsymbalyuk O, Caridi J, Gullapalli RP, Kilbourne MJ, Gerzanich V. MRI evidence that glibenclamide reduces acute lesion expansion in a rat model of spinal cord injury. 2013; 51:823–827.

Simard JM, Popovich PG, Tsymbalyuk O, Gerzanich V. Spinal cord injury with unilateral versus bilateral primary hemorrhage — Effects of glibenclamide. Experimental Neurology. 2012:1–7.

Simard JM, Tsymbalyuk O, Ivanov A, Ivanova S, Bhatta S, Geng Z, Woo SK, Gerzanich V. Endothelial sulfonylurea receptor 1-regulated NCCa-ATP channels mediate progressive hemorrhagic necrosis following spinal cord injury. J Clin Invest. 2007; 117:2105–2113. [PubMed: 17657312]

Simard JM, Woo SK, Norenberg MD, Tosun C, Chen Z, Ivanova S, Tsymbalyuk O, Bryan J, Landsman D, Gerzanich V. Brief Suppression of Abcc8 Prevents Autodestruction of Spinal Cord After Trauma. Science Translational Medicine. 2010; 2:28ra29–28ra29.

Sun F, Lin C-LG, McTigue D, Shan X, Tovar CA, Bresnahan JC, Beattie MS. Effects of axon degeneration on oligodendrocyte lineage cells: dorsal rhizotomy evokes a repair response while axon degeneration rostral to spinal contusion induces both repair and apoptosis. Glia. 2010; 58:1304–1319. [PubMed: 20607865]

Tator CH, Koyanagi I. Vascular mechanisms in the pathophysiology of human spinal cord injury. J Neurosurg. 1997; 86:483–492. [PubMed: 9046306]

Todorich B, Pasquini JM, Garcia CI, Paez PM, Connor JR. Oligodendrocytes and myelination: The role of iron. Glia. 2009; 57:467–478. [PubMed: 18837051]

Tripathi R, McTigue DM. Prominent oligodendrocyte genesis along the border of spinal contusion lesions. Glia. 2007; 55:698–711. [PubMed: 17330874]

Tripathi RB, McTigue DM. Chronically increased ciliary neurotrophic factor and fibroblast growth factor-2 expression after spinal contusion in rats. J Comp Neurol. 2008; 510:129–144. [PubMed: 18615534]

Warden P, Bamber NI, Li H, Esposito A, Ahmad KA, Hsu CY, Xu XM. Delayed glial cell death following wallerian degeneration in white matter tracts after spinal cord dorsal column cordotomy in adult rats. Experimental Neurology. 2001; 168:213–224. [PubMed: 11259109]

Watanabe M, Toyama Y, Nishiyama A. Differentiation of proliferated NG2-positive glial progenitor cells in a remyelinating lesion. J Neurosci Res. 2002; 69:826–836. [PubMed: 12205676]

NIH-PA Author Manuscript

NIH-PA Author Manuscript

NIH-PA Author Manuscript

Yu C-G, Yezierski RP, Joshi A, Raza K, Li Y, Geddes JW. Involvement of ERK2 in traumatic spinal cord injury. Journal of Neurochemistry. 2010; 113:131–142. [PubMed: 20067580]

Zai LJ, Wrathall JR. Cell proliferation and replacement following contusive spinal cord injury. Glia. 2005; 50:247–257. [PubMed: 15739189]

Zhang X, Surguladze N, Slagle-Webb B, Cozzi A, Connor JR. Cellular iron status influences the functional relationship between microglia and oligodendrocytes. Glia. 2006; 54:795–804. [PubMed: 16958088]

Zhu X, Hill RA, Nishiyama A. NG2 cells generate oligodendrocytes and gray matter astrocytes in the spinal cord. NGB. 2008; 4:19.

NIH-PA Author Manuscript

NIH-PA Author Manuscript

NIH-PA Author Manuscript

Highlights

- A rat model of collagenase-induced intraspinal hemorrhage (ISH) was created.
- Macrophages and iron accumulated acutely in lesions and persisted chronically.
- NG2 cells increased and new oligodendrocytes were formed over time after ISH.
- pERK1/2 and pSTAT3 increased acutely after ISH.
- Intraspinal bleeding alone mimics most sequelae of spinal contusion injury.

NIH-PA Author Manuscript

NIH-PA Author Manuscript

NIH-PA Author Manuscript

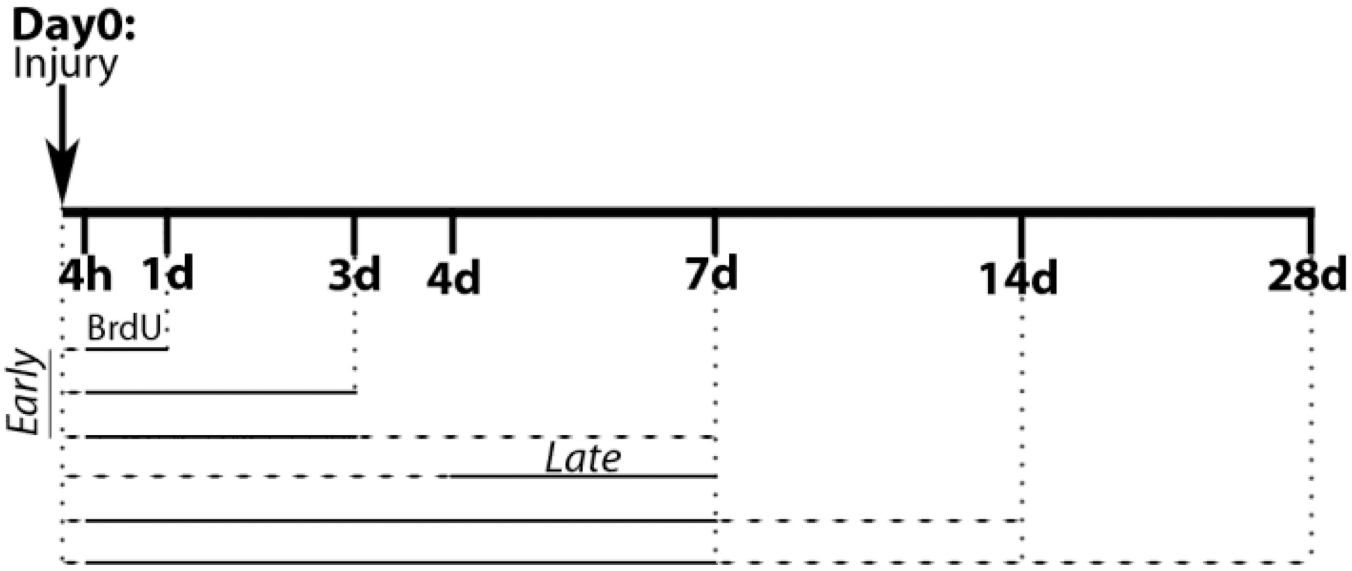

Fig. 1.

Timeline of bromo-deoxyurindine (BrdU) treatment and survival post-injury. BrdU intervals denoted with solid line, time to sacrifice shown with dashed line. Animals sacrificed at 7d post-ISH received BrdU at either early (4h, 1-3d) or late (4-7d) times after injury. Chronic animals (14d and 28d survival) received BrdU 4h after ISH and daily throughout the first week.

NIH-PA Author Manuscript
NIH-PA Author Manuscript
NIH-PA Author Manuscript

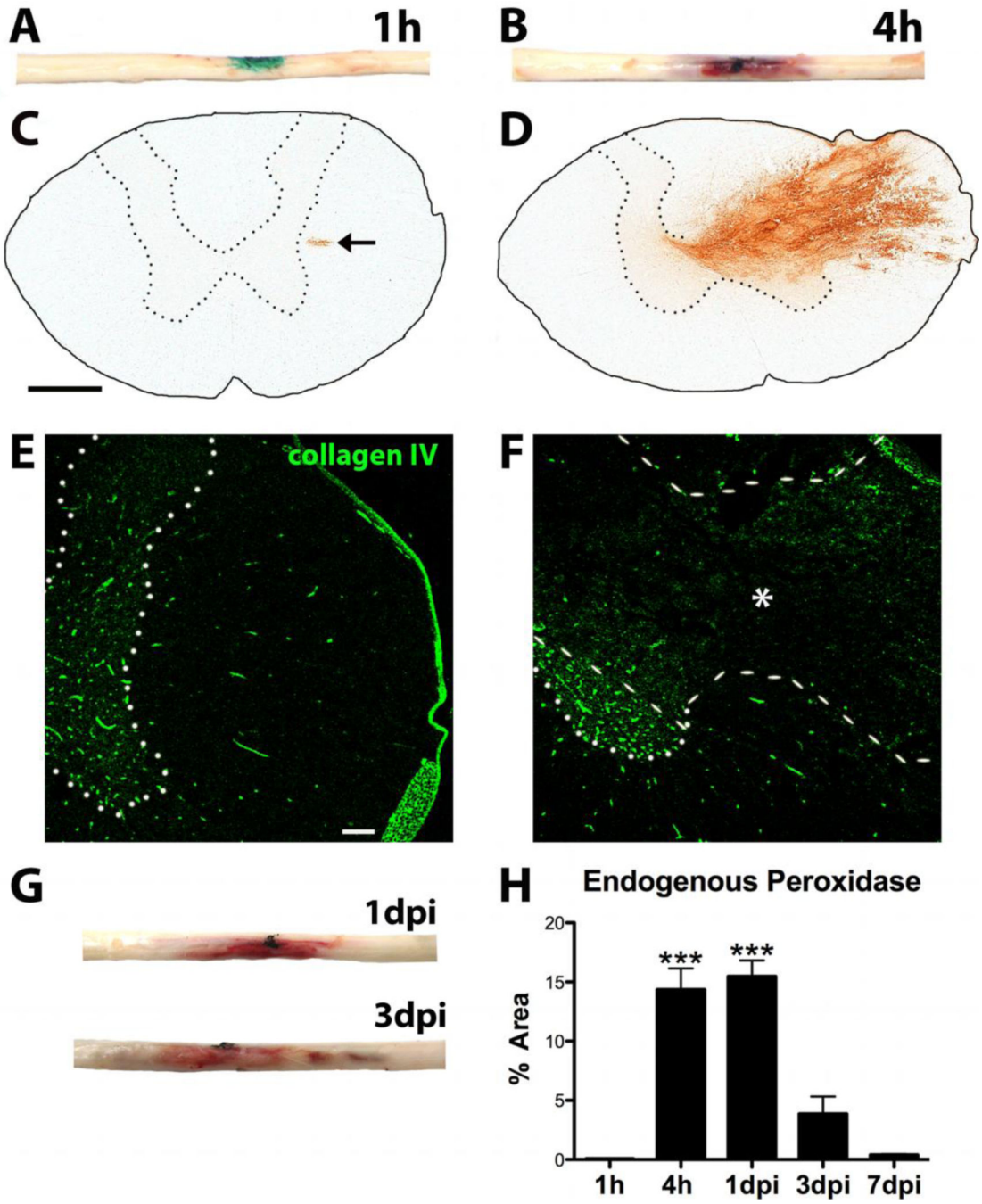

Fig. 2.

Characterization of bleeding and collagen IV breakdown after intraspinal collagenase microinjection. **A**) No overt hemorrhage at 1h in the microinjection site (green) of dissected spinal cords. **B**) Prominent hemorrhage is visible 4h after ISH. Charcoal (black) denotes microinjection site. **C**) Small area of peroxidase reactivity (arrow) is present 1h after ISH. **D**) Blood is clearly visible at 4h as endogenous peroxidase staining (brown) ipsilateral to collagenase injection. **E**) Microvasculature remains intact 1h after ISH, as revealed by collagen IV (green) immunoreactivity. **F**) By 4h after ISH, complete breakdown of

NIH-PA Author Manuscript

NIH-PA Author Manuscript

NIH-PA Author Manuscript

microvasculature within area of hemorrhage is evident by lack of intact collagen IV profiles. Area of hemorrhage denoted by * and outlined with dashed line. Intact gray matter denoted by dotted line in E,F. **G**) Hemorrhage is evident in spinal cords dissected at 1d and 3d after ISH. Charcoal (black) denotes microinjection site. **H**) Proportional area of endogenous peroxidase reactivity is significantly higher at 4h and 1dpi compared to 1h, 3 and 7d post-ISH (*** $p < 0.0001$). Data represent mean ± SEM. Scale bar C 500μm, E 100μm

NIH-PA Author Manuscript
NIH-PA Author Manuscript
NIH-PA Author Manuscript

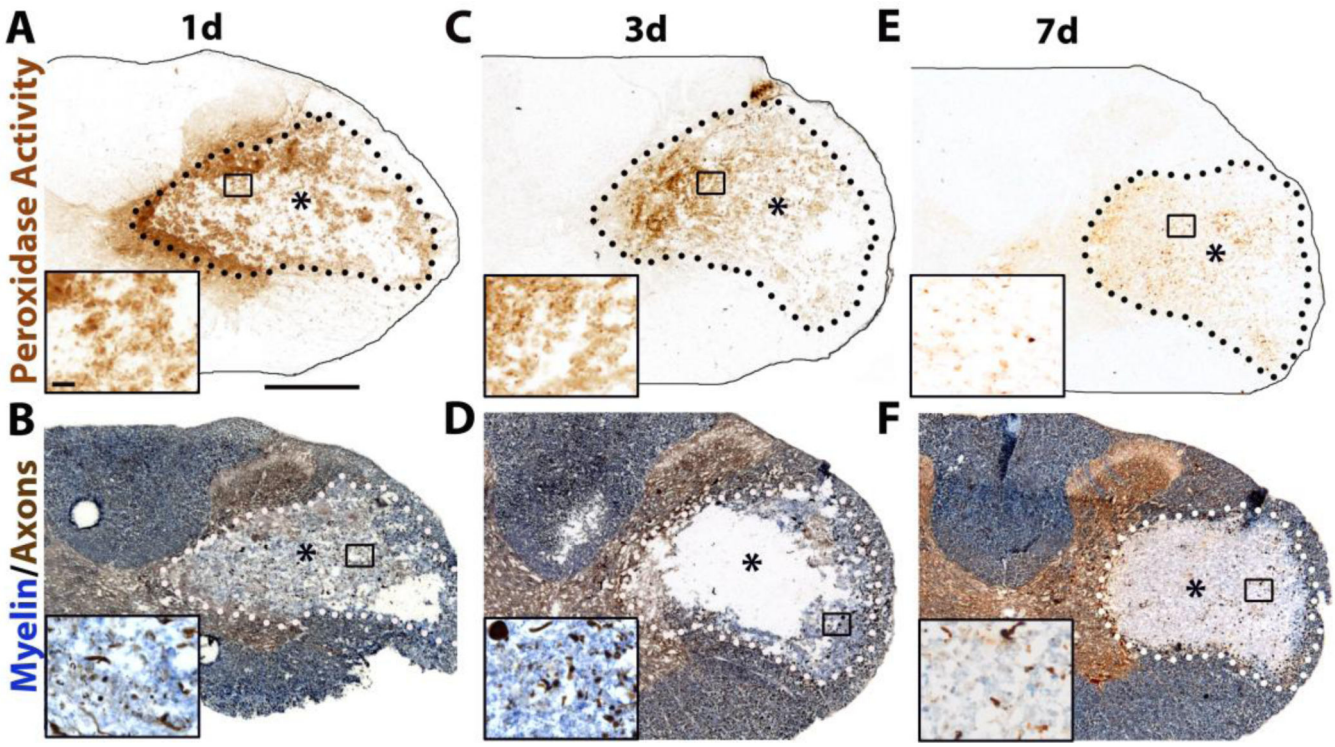

Fig. 3.

Characterization of intraspinal hemorrhage (ISH) model. **A,C,E**) Blood visible within spinal cord as endogenous peroxidase staining at 1d, 3d and 7d post-ISH. **B,D,F**) Eriochrome Cyanine (blue) and neurofilament (brown) labeling show myelin and axons, respectively. Collagenase-induced lesions contain myelin debris, myelin loss, dystrophic axons, and axon loss (lesions denoted by * and dotted line). Boxed areas are shown as high power insets below each image. Scale bar A 500μm, inset 20μm.

NIH-PA Author Manuscript
NIH-PA Author Manuscript
NIH-PA Author Manuscript

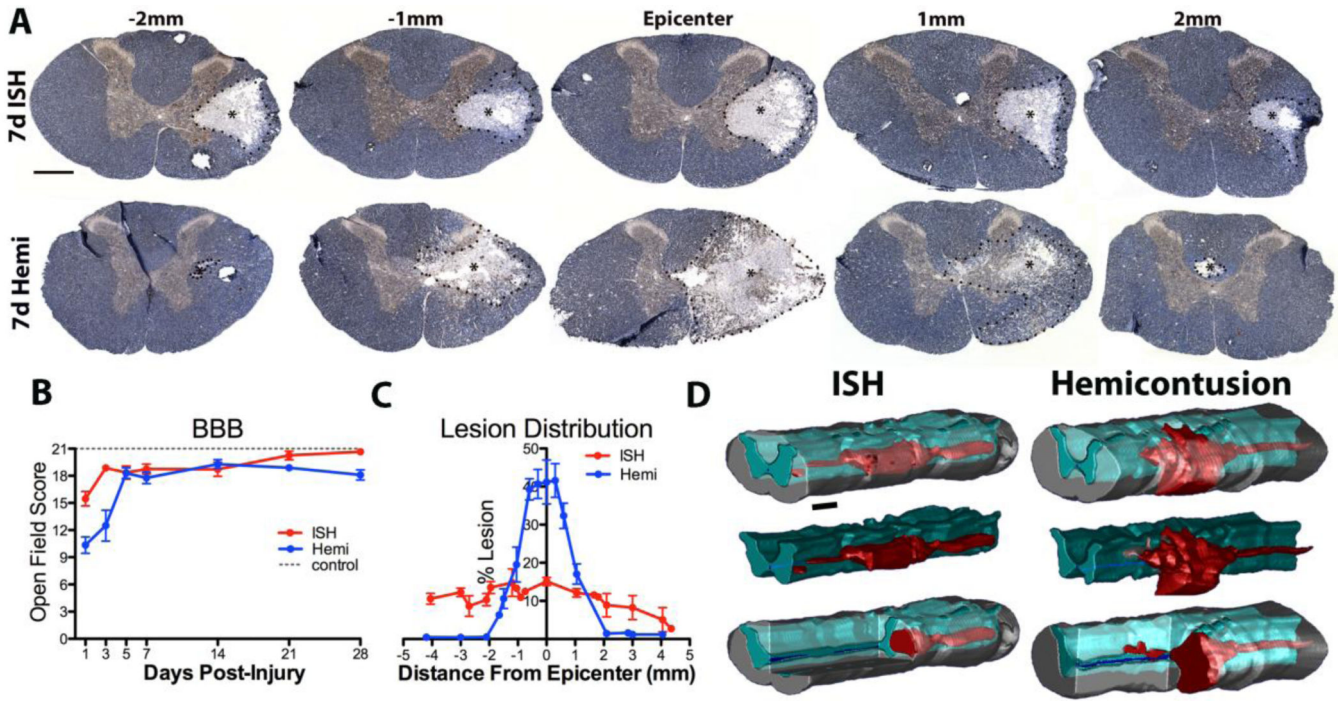

Fig. 4.

Comparison of ISH and hemi-contusion lesions. **A**) Sections are labeled for neurofilament (brown) and myelin (blue). Representative mean lesions (*) from 7dpi rats injured via ISH (top row) or hemi-contusion (bottom row) at the epicenter, and 1mm and 2mm rostral and caudal to the epicenters. **B**) BBB locomotor scores comparing time-course of hindlimb function recovery for ISH (red) and hemi-contusion rats (blue). **C**) Quantification of % lesion areas in cross-sections between 0 to 4.5mm from the epicenter. Length of contusion lesions was ~2mm shorter that ISH lesions. **D**) 3D representation of ISH and hemi-contusion lesions (red), spared gray matter (turquoise) and spared white matter (gray). Data represent mean ± SEM. Scale bar A 500μm, C 1.14mm.

NIH-PA Author Manuscript
NIH-PA Author Manuscript
NIH-PA Author Manuscript

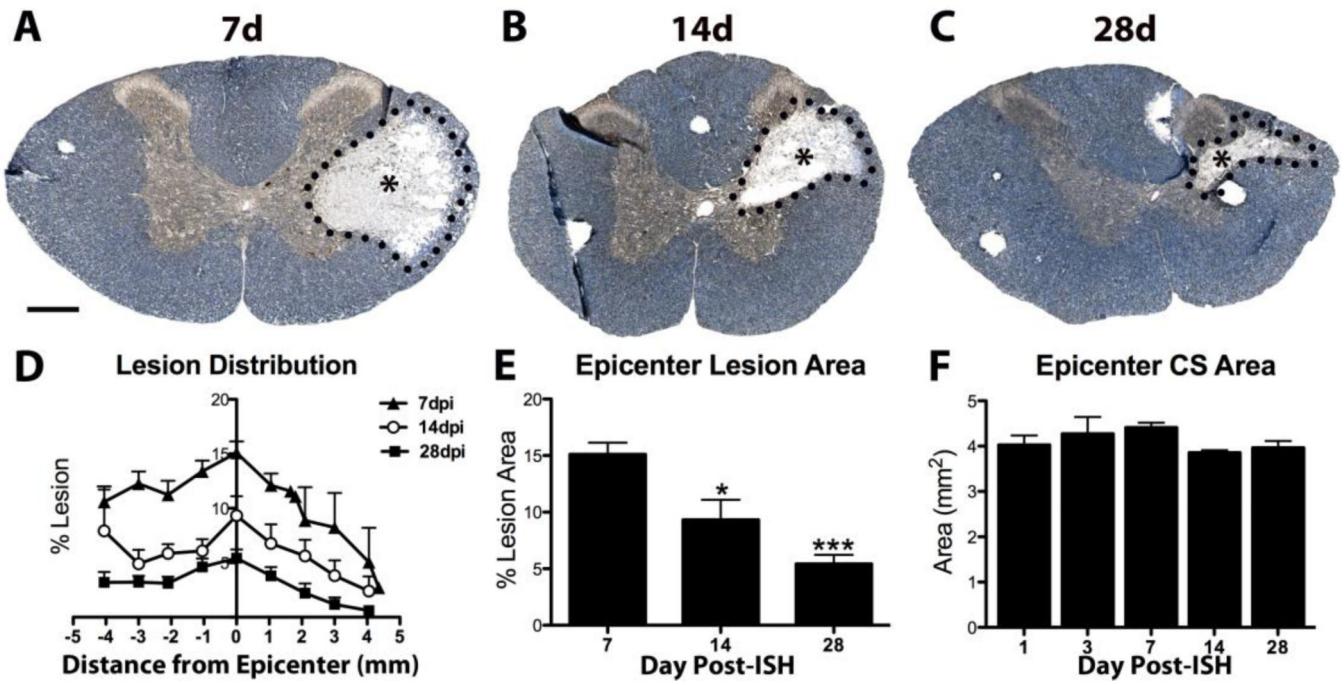

Fig. 5.

Changes in ISH lesion size between 7d – 28d. **A-C**) Sections are labeled for neurofilament (brown) and myelin (blue). Lesion area (* and dotted line) decreased between 7d to 28d. **D**) Quantification of percent total cross-section occupied by lesion. Lesion area decreased from 7 – 28d post-ISH. **E**) Percent lesion area at epicenter decreased significantly at 14d and 28d post-ISH. **F**) Total cross-section (CS) area declined slightly 1 – 28d post-ISH. Data represent mean ± SEM. * $p < 0.05$, *** $p < 0.0001$ vs. 7dpi. Scale bar 500μm.

NIH-PA Author Manuscript

NIH-PA Author Manuscript

NIH-PA Author Manuscript

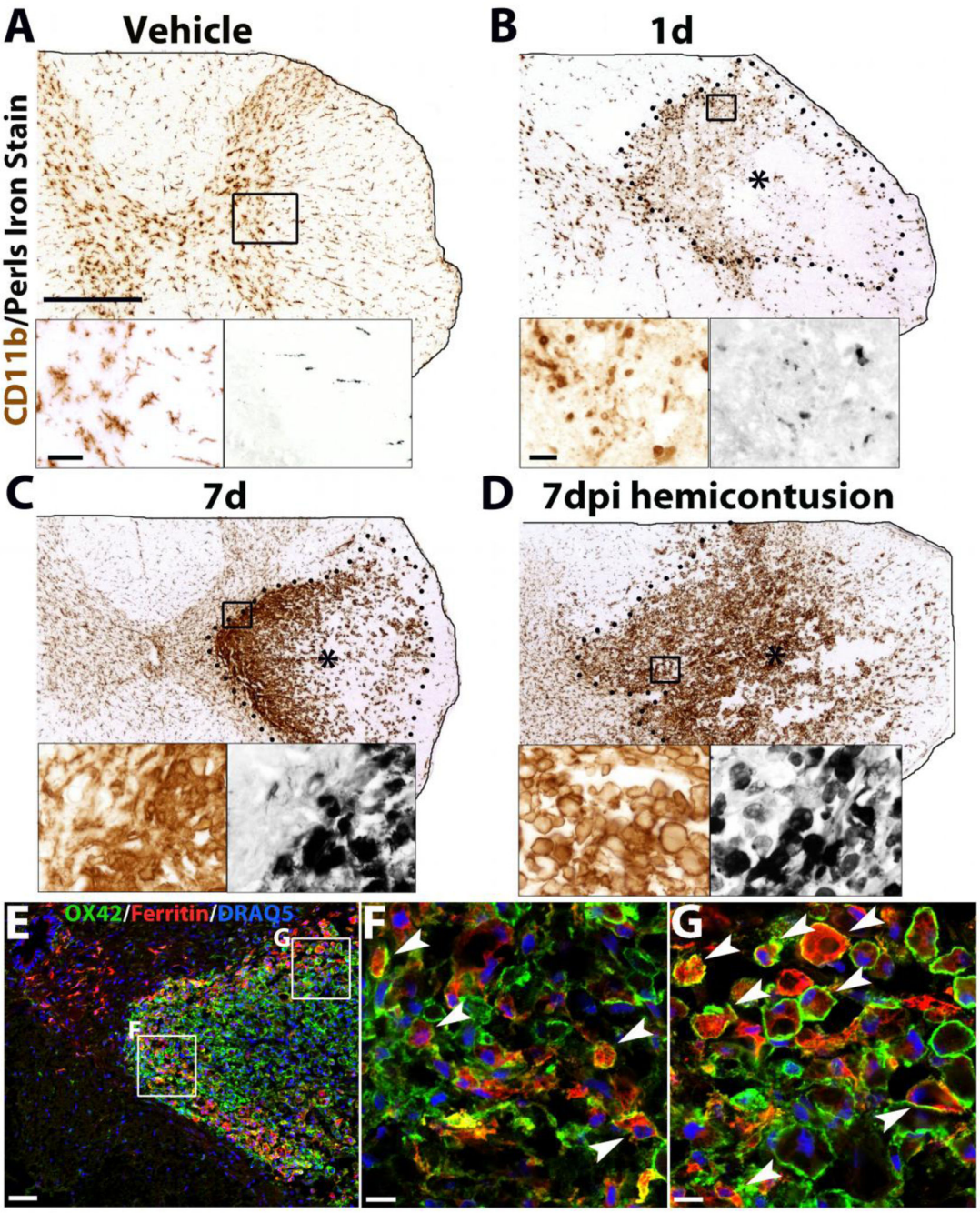

Fig. 6.

Activated macrophages accumulate iron after ISH and Hemi-contusion. **A-D**) Low power images of sections immunolabeled for Cd11b to show microglia and macrophages from control 1d and 7d post-ISH and 7d after hemi-contusion. Boxed areas are shown as high power left insets. Lesions are denoted by * and dotted line. High power views of boxed areas on adjacent sections labeled for iron (Perls) shown on right insets. **E-G**) Confocal images of ferritin (red) and Cd11b (Ox42; green) double-labeling from 7d ISH cords

confirm iron accumulates within macrophages (arrowheads). Sections are counterstained with Draq5. Scale bar A 500μm, A inset 50μm, B-D insets 20μm, E 50μm, F,G 10μm.

NIH-PA Author Manuscript
NIH-PA Author Manuscript
NIH-PA Author Manuscript

NIH-PA Author Manuscript
NIH-PA Author Manuscript
NIH-PA Author Manuscript

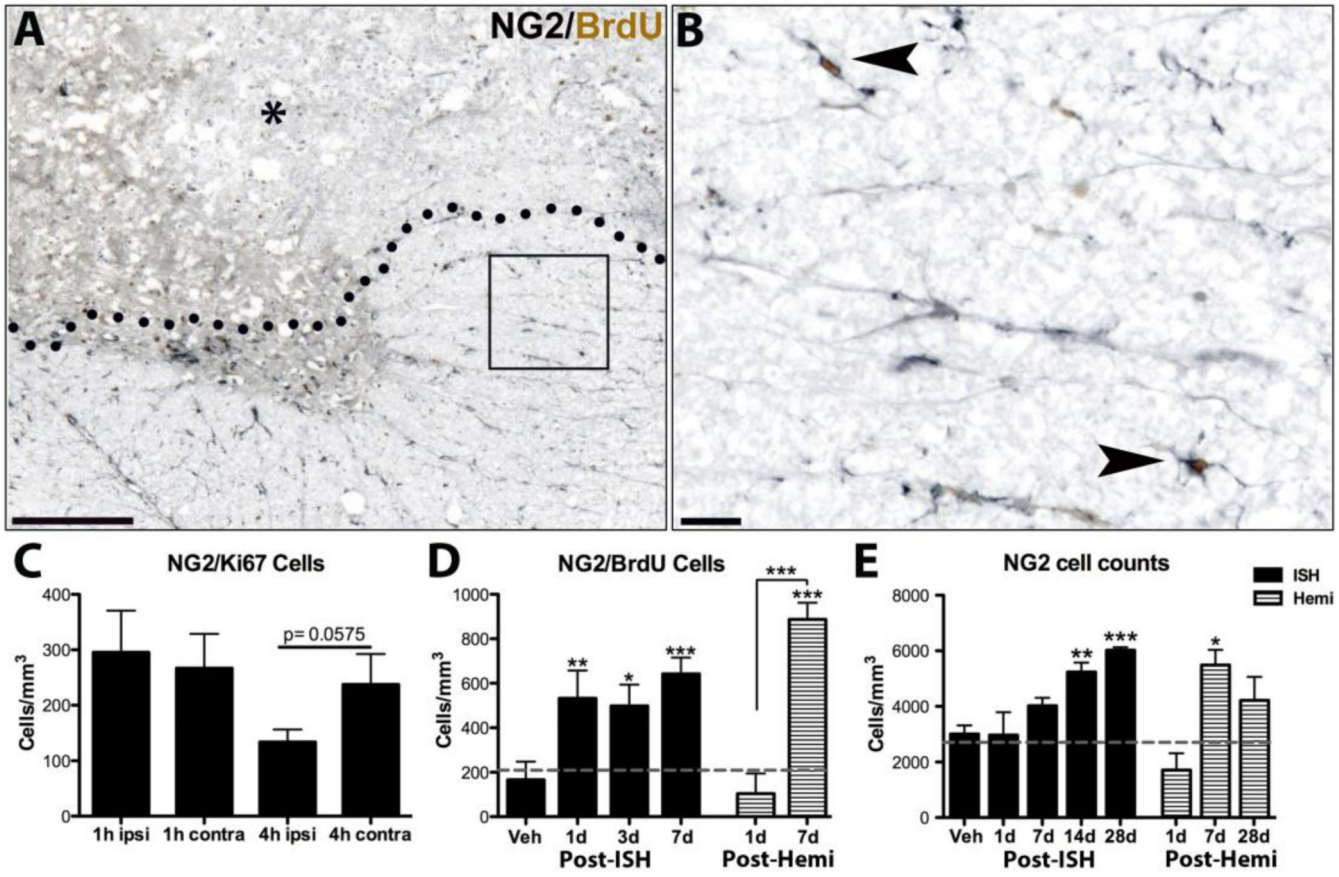

Fig. 7.

NG2 cells proliferate after ISH and hemi-contusion. **A**) Example of NG2/BrdU labeling at 1d post-ISH. BrdU was given at 4h and 22h. Lesion (*) is above dotted line. Boxed area shown at higher power in B). **B**) Two NG2/BrdU positive cells (arrowheads) in spared tissue. **C**) Quantification of ipsilateral and contralateral NG2/Ki67 double-labeled cells acutely after collagenase microinjection (4h ipsi vs. 4h contra, $p < 0.0575$ two-tailed paired t-test). **D**) Quantification of ipsilateral NG2/BrdU cells after ISH or hemi-contusion in rats given BrdU from 4h – 3dpi. **E**) Quantification of total ipsilateral NG2 cells between 1d – 28dpi post-ISH and post-hemi-contusion. *$p < 0.05$, **$p < 0.01$, ***$p < 0.001$ vs. vehicle control (ISH data) or vs. naïve and 1d (post-hemi). Data represent mean ± SEM. Solid bars = ISH; striped bars = hemi- contusion. Number of NG2/BrdU and NG2 cells present in naïve tissue denoted by gray lines (D,E). Scale bar A 500μm, B 50μm.

NIH-PA Author Manuscript
NIH-PA Author Manuscript
NIH-PA Author Manuscript

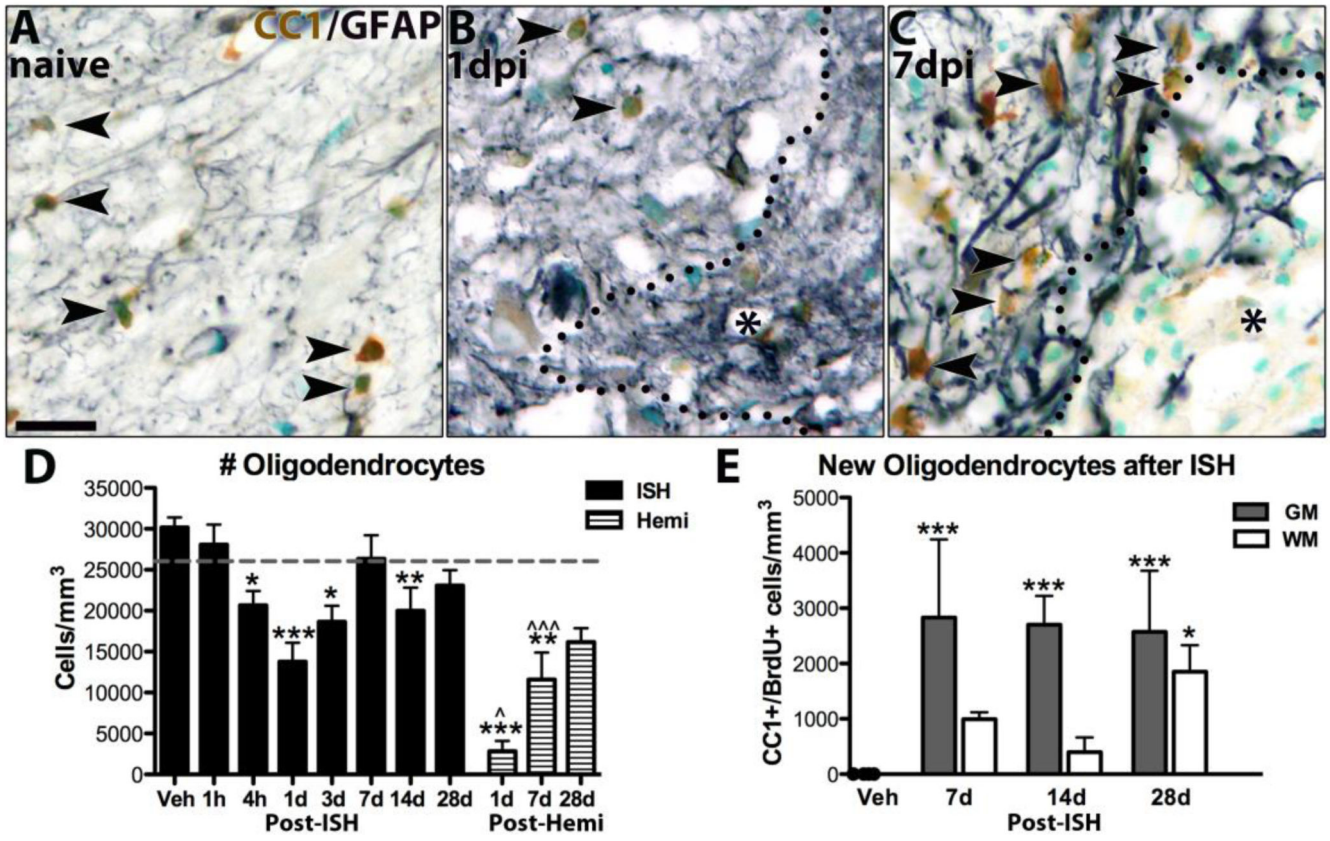

Fig. 8.

New oligodendrocytes replace those lost after ISH and hemi-contusion injuries. **A-C**) Images from gray matter of sections immunolabeled for oligodendrocytes (CC1, brown), astrocytes (gray) and counterstained with methyl green from naïve tissue (A), 1d post-ISH (B) and 7d post-ISH (C). Lesion in B and C denoted by * and black outline. **D**) Oligodendrocytes were quantified ipsilateral to lesions and compared to controls. Oligodendrocyte numbers were significantly reduced 4h, 1d, 3d and 14d after ISH and 1d, 7d after hemi-contusion. Hemi- contusion values are significantly lower than ISH time points at 1d and 7d. **E**) BrdU+ oligodendrocytes were quantified in white matter and gray matter lesion borders in 7d post-ISH tissue from rats receiving BrdU from 4h-3dpi, and from 14d and 28d post-ISH tissue from rats given BrdU 1d-7dpi. Significantly more new oligodendrocytes were present in gray matter at every time, and in white matter at 28d. * $p < 0.05$, **$p < 0.01$, ***$p < 0.001$ vs. control; ^$p < 0.05$, ^^^$p < 0.001$ ISH vs. hemi-contusion. Data represent mean ± SEM. Solid bars = ISH; striped bars = hemi-contusion. Number of oligodendrocytes present in naïve tissue denoted by gray lines (D,E). Scale bar A 20μm.

NIH-PA Author Manuscript

NIH-PA Author Manuscript

NIH-PA Author Manuscript

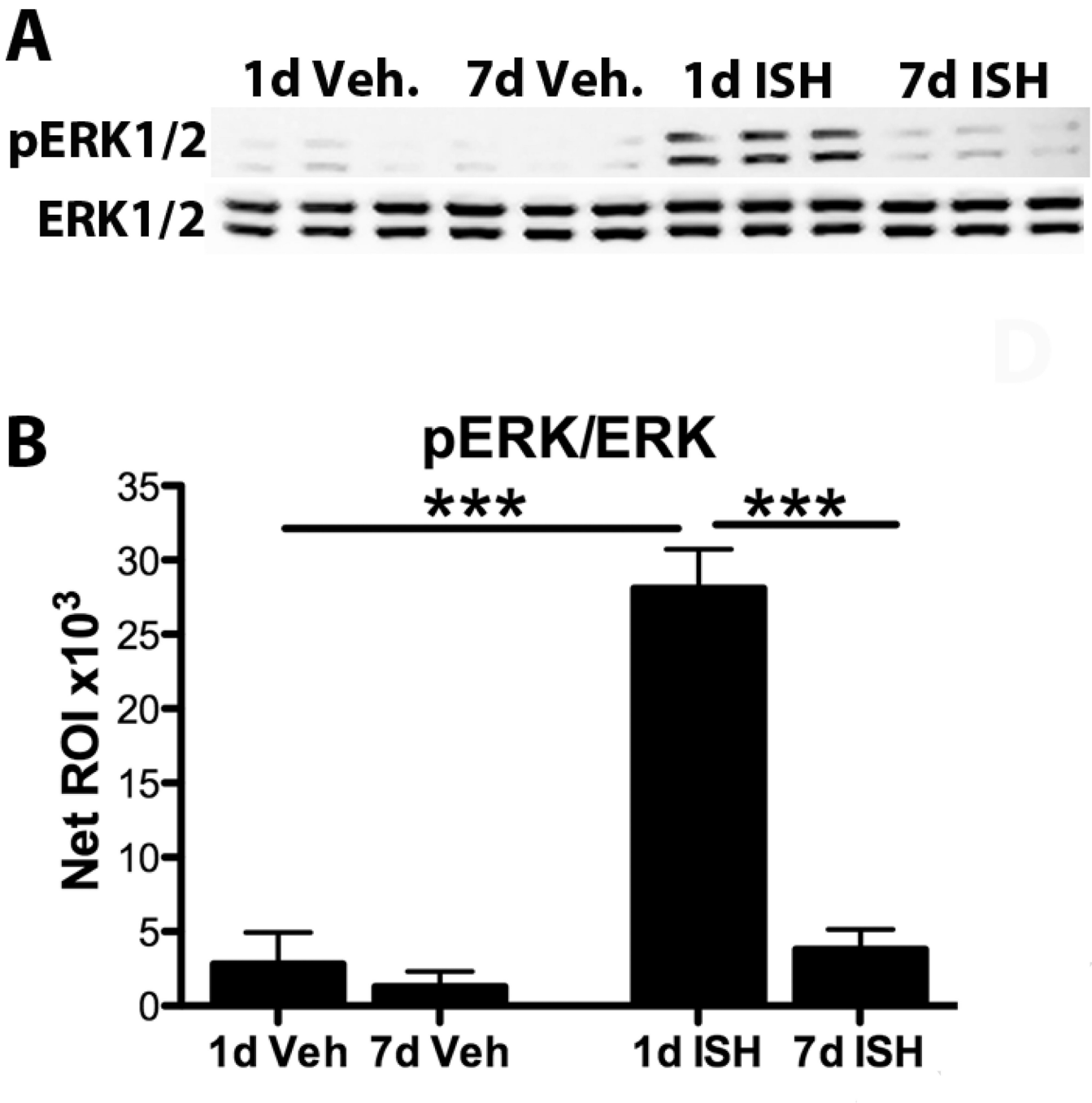

Fig. 9.

ERK1/2 activation is increased acutely after ISH. **A**) Western blot for pERK1/2 and ERK1/2 from protein obtained from injection sites at 1d and 7d after vehicle or collagenase injection **B**) Quantification of bands in A. Significantly more pERK1/2 was present at 1d post- ISH compared to all other groups. ***$p < 0.001$. Data represent mean ± SEM.

NIH-PA Author Manuscript

NIH-PA Author Manuscript

NIH-PA Author Manuscript

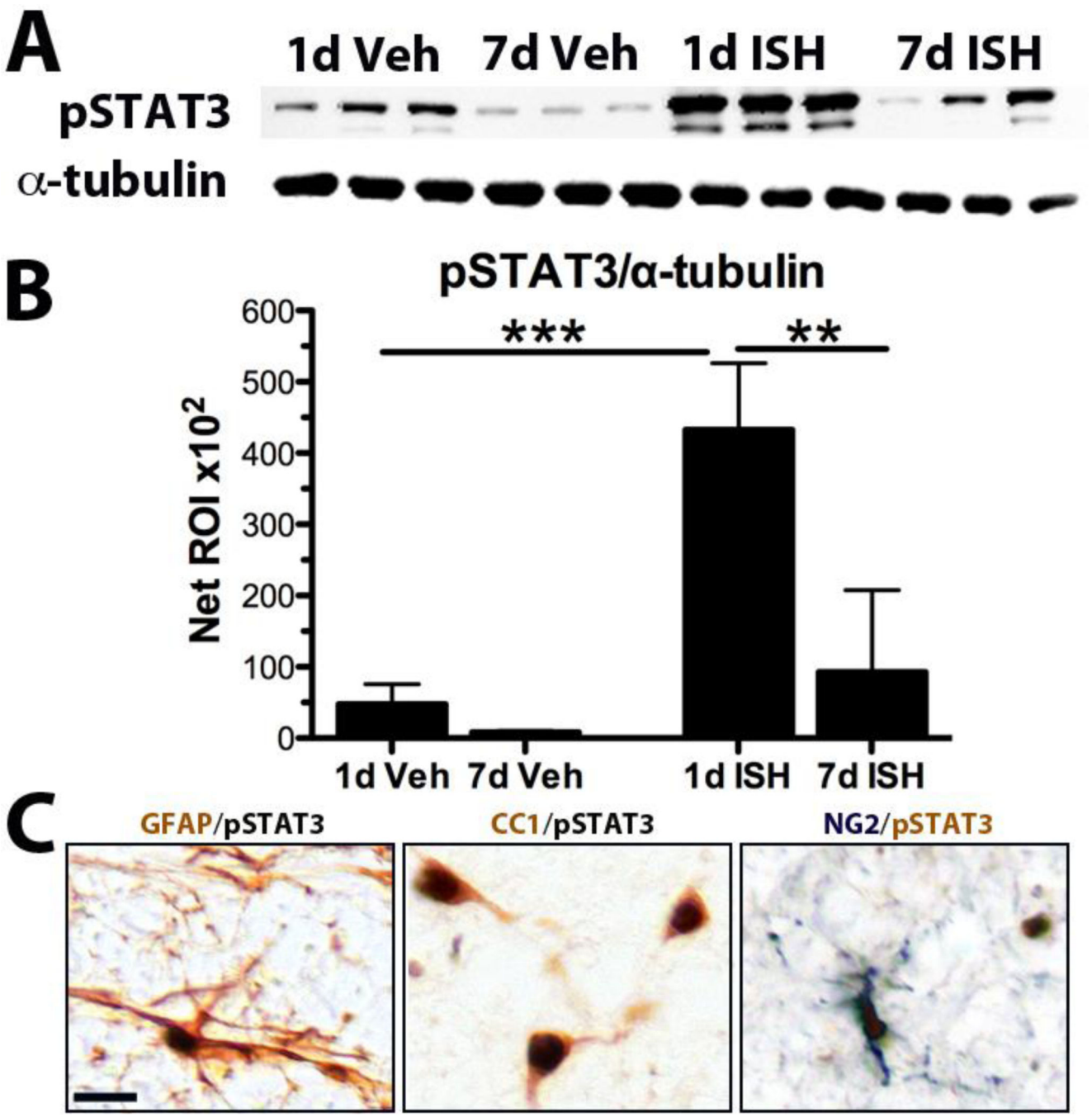

Fig. 10.

STAT3 is activated after ISH. **A**) Western blot for pSTAT3 and α-tubulin (loading control) from protein taken at 1d and 7d after vehicle and 1d and 7d post-ISH. **B**) Quantification of bands in A. Significantly more pSTAT3 was present at 1d post-ISH compared to all other groups. **p < 0.01, ***p < 0.001. Data represent mean ± SEM. **C**) 1d post-ISH tissue. Examples of pSTAT3+ double-labeling with a GFAP+ astrocyte, CC1+ oligodendrocytes, and an NG2+ oligodendrocyte progenitor cell (arrowheads). Scale bar 20μm.

NIH-PA Author Manuscript
NIH-PA Author Manuscript
NIH-PA Author Manuscript

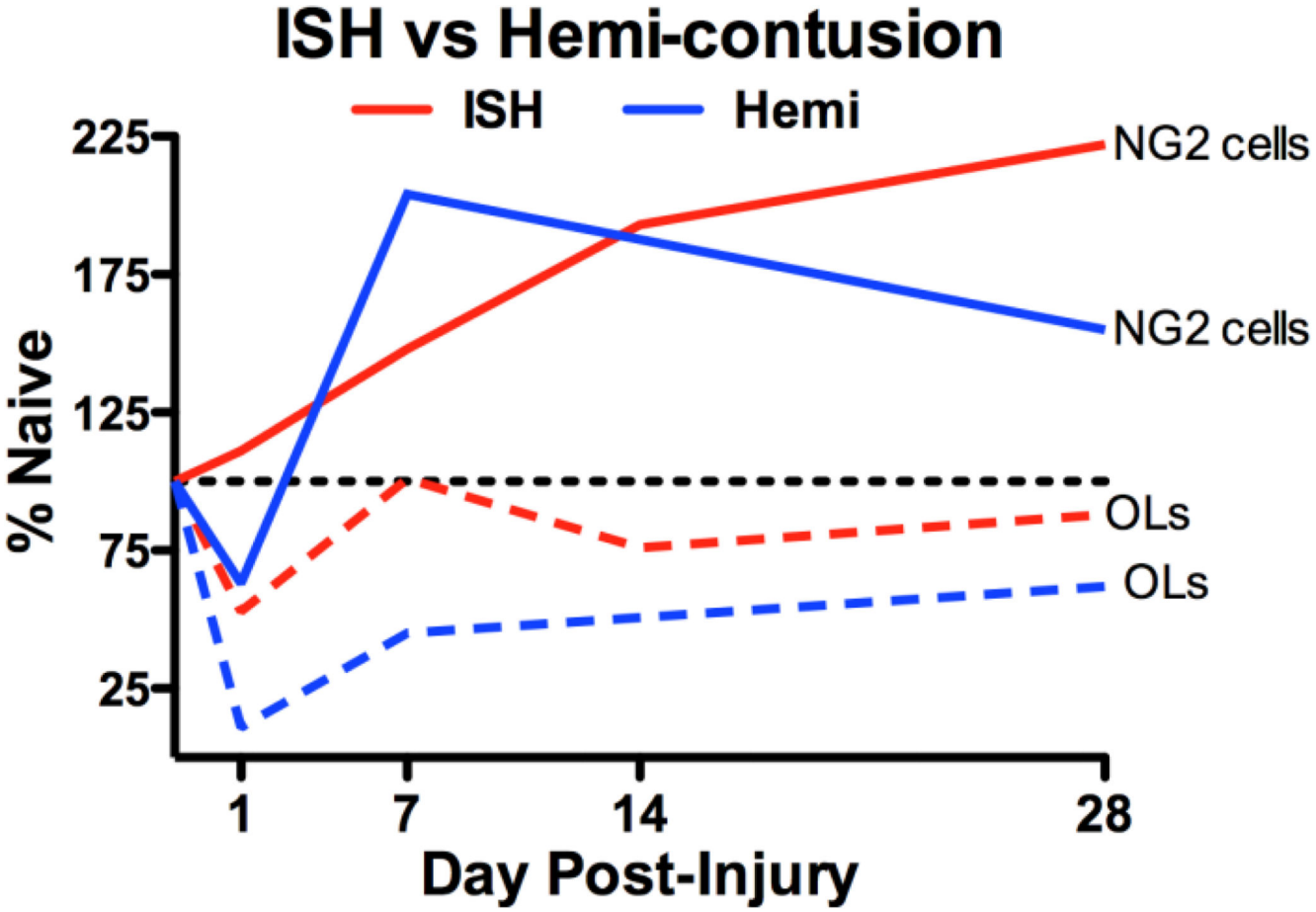

Fig. 11.

Comparison of NG2 cell and oligodendrocyte numbers after ISH (red) and hemi- contusion (blue). NG2 cells (solid lines) show slightly altered patterns in the first week post- injury and overall plateau higher than controls. Oligodendrocytes (dashed lines) are lost by 1d post-injury in both models and rise over the next several weeks.

NIH-PA Author Manuscript

NIH-PA Author Manuscript

NIH-PA Author Manuscript

TABLE 1

Experimental Groups and BrdU Regimen

Group	Sacrifice (dpi)	BrdU Regimen	n
naïve	4	4d pre-perfusion	4
collagenase	1h	Immediately post-microinjection	5
collagenase	4h	1h	5
saline control	1	4h, 1dpi	3
collagenase	1	4h, 1dpi	5
collagenase	3	4h, 1-3dpi	3
collagenase	7	4h, 1-3dpi	3
collagenase	7	4-7dpi	5
saline control	7	4h, 1-3dpi	4
collagenase	14	4h, 1-7dpi	5
collagenase	28	4h, 1-7dpi	4
Hemi-contusion	1	4h, 1dpi	5
Hemi-contusion	7	4h, 1-3dpi	6
Hemi-contusion	28	4h, 1-7dpi	5

NIH-PA Author Manuscript

NIH-PA Author Manuscript

NIH-PA Author Manuscript

TABLE 2

Comparison of Post-Injury NG2 Cell and Oligodendrocyte (OL) Dynamics

Model	Day post-injury	Mean #OLs	Mean # NG2 cells	Mean OL/NG2 cell ratio
Uninjured control[+]	---	260	27	10.7
ISH	1d	138	30	4.7**
	7d	263	40	4.0**
	28d	228	60	3.7**
Hemi-contusion	1d	28	17	1.4*** ^
	7d	116	55	2.6***
	28d	162	42	3.8**

[+]Values for uninjured controls were not different from vehicle controls in ISH group.

** $p<0.01$ vs. Uninjured control;

*** $p<0.001$ vs. Uninjured control

^ $p<0.05$ 1d Hemi-contusion vs. 1d ISH